Digital Signal Processing 120 (2022) 103246

Contents lists available at ScienceDirect

Digital Signal Processing

www.elsevier.com/locate/dsp

Third-order Volterra MMSE receivers for enhanced single and multiple antenna interference cancellation

Mustapha Sadok [a], Jean-Pierre Delmas [b,*], Pascal Chevalier [c,d]

[a] Institut National des telecommunications et des Technologies de l'Information et de la Communication (INTTIC), and LaRATIC laboratory, BP 1518 Oran El M'nouer Oran 31000, Algeria
[b] Samovar lab, Telecom SudParis, Institut Polytechnique de Paris, 91011 Evry Cedex, France
[c] CNAM Cedric laboratory, Hesam University, 292 rue Saint Martin, 75003 Paris, France
[d] Thales SIX GTS France, HTE/AMS/TCP, 92622 Gennevilliers Cedex, France

ARTICLE INFO

Article history:
Available online 14 September 2021

Keywords:
Non-linear
Non-Gaussian
Non-circular
Widely linear, third-order Volterra
SAIC
MMSE

ABSTRACT

Data-like interference mitigation in wireless communications systems, and in mobile cellular networks in particular, has always been a challenging problem which is becoming even more so for 5G networks and beyond including the Internet of things (IoT), to support a massive number of low data rate devices for given spectral resources. A promising solution to this problem consists in using one dimensional signaling (i.e., real-valued modulations) jointly with widely linear (WL) processing at the receiver, which has the capability to process up to $2N-1$ data-like interference from N antenna receivers, and to fulfill, for $N=1$, single antenna interference cancellation (SAIC) of a one-dimensional interference in particular. However, when the signal of interest (SOI) and observations are jointly non-Gaussian, which is the case for most of digital radiocommunications systems, WL receivers become sub-optimal and optimal receivers become non-linear. It is then of interest to propose new non-linear receivers to improve performance of WL receivers. In this context, the paper aims at introducing, for small-scale systems, third-order complex Volterra (CV) minimum mean square error (MMSE) receivers, for the reception of a digital linearly modulated SOI whose waveform is known, corrupted by potentially non-Gaussian and non-circular interference, omnipresent in practical situations. Properties, performance and adaptive implementation of these receivers in the presence of non-Gaussian and potentially non-circular interference up to the 6th-order are analyzed in this paper. In particular, some of these receivers are shown to enhance WL receiver performance for SAIC of one rectilinear interference such as binary phase-shift keying (BPSK) interference. Whereas some other receivers allow us to fulfill SAIC of 4th-order non-circular interference such as quadrature phase-shift keying (QPSK) interference, which is not possible using WL receivers. These new receivers open new perspectives for cancellation of non-Gaussian and potentially non-circular interference up to 6th-order in radiocommunication networks.

1. Introduction

Data-like interference mitigation in wireless communications systems, and in mobile cellular networks in particular, has always been a challenging problem which is becoming even more so for 5G networks and beyond, including the IoT, to support a massive number of low data rate devices for given spectral resources. A promising solution to this problem consists in using one dimensional signaling (i.e., real-valued modulations) jointly with WL processing at the receiver [1], which has the capability to process up to $2N-1$ data-like interference from N antenna receivers, and to fulfill, for $N=1$, SAIC of a one-dimensional interference in particular [2–4]. Extension of the SAIC concept to multiple antennas is called multiple antenna interference cancellation (MAIC). Let us recall that one-dimensional modulations are also called rectilinear (R) modulations and correspond, for example, to BPSK or amplitude shift keying (ASK) modulations.

However WL receivers are only optimal when the SOI and observations are zero-mean, jointly Gaussian and non-circular [5]. When the SOI and observations are jointly non-Gaussian, WL receivers then become sub-optimal and optimal receivers have a more general

* Corresponding author.
E-mail addresses: msadok@inttic.dz (M. Sadok), jean-pierre.delmas@it-sudparis.eu (J.-P. Delmas), pascal.chevalier@cnam.fr (P. Chevalier).

https://doi.org/10.1016/j.dsp.2021.103246
1051-2004/

non-linear structure. Such situations are omnipresent in practice. Indeed, most of digital communications signals are non-Gaussian and many of them are non-circular either at the second order (SO) and/or at a higher order (HO). For example, an ASK signal is non-Gaussian and at least non-circular at all even orders. A phase shift keying signal with M states (M-PSK) is non-Gaussian and non-circular at an order $2q$ such that $2q \geq M$ [6]. A square quadrature amplitude modulated (QAM) signal with $4M^2$ states ($4M^2$-QAM) is non-Gaussian and at least fourth-order (FO) non-circular. In this context, it becomes to interest to propose new non-linear receivers to improve performance of WL receivers.

More precisely, when the SOI and observations are jointly non-Gaussian (jointly circular or not), the optimal receiver becomes a non-linear function of the observations, which depends on the joint probability distribution of the SOI and the observed data. However in practice, this probability distribution is generally not known a priori. A first philosophy then consists in trying to estimate it in order to optimize the non-linearity of the receiver. This estimation may be implemented through stochastic techniques, based, for example, on particle filtering [7,8] or through a parametric model of the non-Gaussian observations, such as the Gaussian mixture model [9], well-suited to modelize non-Gaussian/non-circular noise [10]. However, in all cases, this philosophy is generally costly and difficult to implement. A second philosophy, much easier to implement, consists in imposing a particular non-linear structure to the receiver, including the linear one, and to compute a MMSE receiver having this imposed structure. Although sub-optimal, this receiver is built to generate a performance improvement with respect to the linear one in non-Gaussian contexts. A particular non-linear structure, including both the linear and the WL structures, corresponds to the pth-order ($p \geq 2$) complex Volterra structure [11,12]. Such a structure is able to improve the performance of linear receivers in non-Gaussian and potentially non-circular contexts, by exploiting both the non-Gaussiannity and the complete potential non-circularity of the observations up to the order $2p$. Note that research to reduce computational complexity of Volterra filtering is still active (see e.g., [13]). Let us recall that Volterra filtering [14] has been considered in signal processing for a long time for many applications such as for example detection and estimation [15], system identification [16], echo cancellation [17] or non-linear channel equalization [18] but mainly for real-valued observations. The main use of Volterra filtering for complex data concerns both the modeling and the predistortion processing of the baseband input-output relationship of power amplifiers operating close to saturation for power efficiency in radiocommunications [19,20]. The scarce other works about complex Volterra filtering mainly concern blind identification of some linear-quadratic systems [21], mean square estimation and detection from linear-quadratic [22] or pth-order systems [11,12] and beamforming [23–25]. [23] introduces a particular third-order Volterra MVDR beamformer for non-Gaussian interference rejection improvement. However, this beamformer requires a multiple antenna reception, does not include the WL structure, does not take into account the potential non-circularity of the interference and may generate lower performance than the WL beamformers. In contrast, [24] and [25] introduce more general third-order Volterra beamformers, exploiting both the non-Gaussiannity and the potential non-circularity of the interference. However [24] concerns coded division multiple access (CDMA) cellular networks, whereas [25] requires a multiple antenna reception and exploits the potential non-circularity of the interference only. Note that the FO non-circularity of observations has been used by a WL MMSE beamformer in [26] to compensate I/Q imbalance effects at reception but not to improve the steady-state performance of WL beamformers. In addition, the non-Gaussiannity and both the sub-Gaussiannity and non-circularity of observations have already been used in [27] and [28] respectively, through the development of the linear minimum dispersion beamformer (MDB) and the WL MDB respectively, to boost the convergence speed of linear and WL beamformers respectively, but not to improve their steady-state performance. Finally note that some preliminary results of the paper have been presented in [29].

In this context, the first purpose of this paper is to introduce several third-order Volterra MMSE receivers for the reception of a digital linearly modulated SOI, whose waveform is known, corrupted by potentially non-Gaussian and non-circular interference. All these receivers are third-order extensions of the linear MMSE receiver, whereas some of them are third-order extensions of the WL MMSE receiver [2,30,31]. All the proposed receivers exploit the potential non-Gaussian nature of the interference, whereas some of them exploit, in addition, their non-circularity up to order 4 or 6. It is important to note that the proposed receivers have no interest for large-scale systems, such as massive multiple-input and multiple-output (MIMO) systems for 5G mobile cellular networks, for which the linear receivers are quasi-optimal since the sources can be assumed to be approximately orthogonal to each other for the array. On the contrary, the proposed receivers are mainly developed for small-scale systems, with a small number of antennas and low spatial aperture in number of wavelengths, which are low spatial resolution systems for which the linear MMSE receiver has limited performance in the presence of interference. For such systems the idea is to replace the missing hardware (or antennas) by clever software with a moderate complexity, to improve the interference cancellation. The analysis of the properties, performance in terms of signal to interference plus noise ratio (SINR) and symbol error rate (SER), and adaptive implementation of the proposed third-order receivers constitute the second purpose of this paper. In particular, some of these receivers are shown to enhance WL receivers performance for SAIC of one rectilinear interference, whereas some other receivers allow us to fulfill SAIC of 4th-order non-circular interference such as QPSK interference, result which is not possible from WL receivers. These new receivers open new perspectives for cancellation of non-Gaussian and potentially non-circular interference up to 6th-order in radiocommunication networks.

The paper is organized as follows. After the introduction of some hypotheses, data statistics and problem formulation are given in Section 2. Enlightening interpretations and related generic output (SINR) performance of the Mth-order CV MMSE receiver are given in Section 3. Then the new third-order Volterra MMSE receivers are introduced. An analytical performance analysis with SINR and SER illustrations at the output of some of the proposed MMSE receivers is presented in Sections 4 and 5 in the presence of one and two interferences, respectively. An adaptive implementation and a complexity analysis of the proposed receivers are briefly investigated in Section 6. Finally Section 7 concludes this paper.

The following notations are used throughout the paper. Matrices and vectors are represented by bold upper case and bold lower case characters, respectively. Vectors are by default in column orientation, while T, H and $*$ stand for transpose, conjugate transpose and conjugate, respectively. E(.) is the expectation operator and $\star$ is the convolution product. $\otimes$ and $\oslash$ denote, respectively, the usual Kronecker product and the symmetric Kronecker product between identical vectors that contains only all the distinct products of their components to avoid any redundancies. $\mathbf{a}^{\oslash q}$ means $\mathbf{a} \oslash \mathbf{a} \ldots \oslash \mathbf{a}$ with $q-1$ symmetric Kronecker products.

2. Hypotheses, data statistics and problem formulation

2.1. Hypotheses

We consider an array of N narrow-band antennas receiving the contribution of an SOI corrupted by interferences and a background noise. Assuming propagation channels with no delay spread and perfect time and frequency synchronization of the SOI, which are acceptable hypotheses for example for some satellite communication applications [32], the complex envelope of the observation vector at the output of the antennas can then be written as

$$\mathbf{x}(t) = \mu_s \sum_k a_k v(t-kT)\mathbf{h}_s + \sum_{p=1}^{P} j_p(t)\mathbf{h}_{j_p} + \mathbf{n}(t) \in \mathbb{C}^N, \tag{1}$$

where a_k are zero-mean i.i.d. random variables corresponding to the symbols of the SOI, $j_p(t)$ are zero-mean and potentially non-Gaussian and/or non-circular co-channel interferences (CCI), and $\mathbf{n}(t)$ is the background noise, assumed to be zero-mean, Gaussian, stationary, circular and spatially white. The random variables a_k, $j_p(t), p = 1, \ldots, P$ and $\mathbf{n}(t)$ are independent to each other. T is the symbol period and $v(t)$ is the impulse response of the pulse shaping filter of the SOI whose μ_s controls its amplitude. $\mathbf{h}_s$ and $\mathbf{h}_{j_p}$ are the channel vectors (whose module of the first component is unity) of the SOI and CCI, respectively. Assuming that $v(t)$ is a raised cosine 1/2 Nyquist filter and denoting by $\mathbf{x}_k$ the sampled observation, at the symbol rate, at time kT at the output of a matched filtering operation to the pulse shaping filter, we obtain:

$$\mathbf{x}_k = \mu_s a_k r(0)\mathbf{h}_s + \sum_{p=1}^{P} j_{p,k}\mathbf{h}_{j_p} + \mathbf{n}_k, \tag{2}$$

where $r(t) \overset{\text{def}}{=} v(t) \star v^*(-t)$ is the real-valued impulse response of a Nyquist filter, whereas $j_{p,k}$, for $p = 1, \ldots, P$ and $\mathbf{n}_k$ are respectively the CCI and background noise contribution at the output of the matched filter sampled at symbol rate. The sequences $j_{p,k}, p = 1,_l \ldots, P$ are assumed stationary to the second-order. Consequently, the components of $\mathbf{n}_k$ are zero-mean, spatially white, Gaussian and circular with power η_2. If a'_k and $j'_{p,k}$ denote the normalized SOI symbols and CCI, respectively, such that $\mathrm{E}|a'^2_k| = \mathrm{E}|j'^2_{p,k}| = 1$, (2) takes the form

$$\mathbf{x}_k = \sqrt{\pi_s}a'_k\mathbf{h}_s + \sum_{p=1}^{P} \sqrt{\pi_{j_p}}j'_{p,k}\mathbf{h}_{j_p} + \mathbf{n}_k, \tag{3}$$

where $\pi_s \overset{\text{def}}{=} \mu_s^2\pi_a r^2(0)$ with $\pi_a \overset{\text{def}}{=} \mathrm{E}|a_k^2|$ and $\pi_{j_p} \overset{\text{def}}{=} \mathrm{E}|j_{p,k}^2|$.

2.2. Data statistics

2.2.1. Presentation

To study the statistical performance of the third-order Volterra MMSE receivers, we need to introduce the SO, FO and sixth-order (SIO) statistics of the SOI and CCI. If u_k denotes the normalized SOI or CCI components, the real-valued FO and SIO circular statistics of u_k assumed second-order stationary, are respectively

$$\kappa_{u,c} \overset{\text{def}}{=} \mathrm{E}|u_k^4| \ \text{ and } \ \chi_{u,c} \overset{\text{def}}{=} \mathrm{E}|u_k^6| \tag{4}$$

and the generally complex-valued SO, FO and SIO non-circular statistics of u_k are respectively

$$\gamma_u \overset{\text{def}}{=} \mathrm{E}(u_k^2), \ \ \kappa_{u,nc,i} \overset{\text{def}}{=} \mathrm{E}(u_k^{5-i}u_k^{*(i-1)}), i = 1, 2 \ \text{ and } \ \chi_{u,nc,i} \overset{\text{def}}{=} \mathrm{E}(u_k^{7-i}u_k^{*(i-1)}), i = 1, 2, 3. \tag{5}$$

2.2.2. Particular cases

To be able to quantify and illustrate the performance of the proposed third-order Volterra MMSE receivers that are presented in Sections 4 and 5, we consider hereafter three particular cases of CCI $j_p(t)$.

In the first case, $j_p(t)$ corresponds to the complex envelope of a digital linearly modulated signal, defined by:

$$j_p(t) = \mu_{j_p} \sum_\ell b_{p,\ell} v(t - \ell T - \tau_{j_p}), \tag{6}$$

where $b_{p,\ell}$ are i.i.d. zero-mean CCI symbols, $\tau_{j_p} \in [0, T)$ is the delay of the CCI w.r.t. the SOI and μ_{j_p} controls the amplitude of the CCI. In this case, the samples $j_{p,k}$ in (2) become

$$j_{p,k} = \mu_{j_p} \sum_\ell b_{p,\ell} r((k-\ell)T - \tau_{j_p}) = \sqrt{\pi_{j_p}}j'_{p,k}, \tag{7}$$

where $\pi_{j_p} = \mu_{j_p}^2 \mathrm{E}|b_{p,\ell}^2| \left(\sum_\ell r^2((k-\ell)T - \tau_{j_p})\right)$. The expressions of the SO, FO and SIO statistics of $j'_{p,k}$ depend on the nature of the symbols $b_{p,\ell}$. For real-valued symbols, $\gamma_{j_p} = 1$ and the FO and SIO statistics reduce to

$$\kappa_{j_p} \overset{\text{def}}{=} \mathrm{E}(j'^4_{p,k}) = \mathrm{E}(b^4_{p,k}) \sum_{\ell} r^4_{p,\ell} + 6[\mathrm{E}(b^2_{p,k})]^2 \sum_{j<\ell} r^2_{p,j} r^2_{p,\ell} \tag{8}$$

$$\chi_{j_p} \overset{\text{def}}{=} \mathrm{E}(j'^6_{p,k}) = \mathrm{E}(b^6_{p,k}) \sum_{\ell} r^6_{p,\ell} + 30\mathrm{E}(b^2_{p,k})\mathrm{E}(b^4_{p,k}) \sum_{j<\ell} r^4_{p,j} r^2_{p,\ell} + 90[\mathrm{E}(b^2_{p,k})]^3 \sum_{i<j<\ell} r^2_{p,i} r^2_{p,j} r^2_{p,\ell}, \tag{9}$$

where $r_{p,i} \overset{\text{def}}{=} r(iT - \tau_{j_p}) / \sqrt{\mathrm{E}|b^2_{p,k}| \sum_{\ell} r^2(\ell T - \tau_{j_p})}$. For symmetric (w.r.t. the origin) SO circular symbols, we obtain:

$$\begin{aligned}
\kappa_{j_p,c} &= \mathrm{E}|b^4_{p,k}| \sum_{\ell} r^4_{p,\ell} + 4[\mathrm{E}|b^2_{p,k}|]^2 \sum_{j<\ell} r^2_{p,j} r^2_{p,\ell} \\
\kappa_{j_p,nc,1} &= \mathrm{E}(b^4_{p,k}) \sum_{\ell} r^4_{p,\ell} \\
\kappa_{j_p,nc,2} &= \mathrm{E}(b^2_{p,k}|b^2_{p,k}|) \sum_{\ell} r^4_{p,\ell}
\end{aligned} \tag{10}$$

$$\begin{aligned}
\chi_{j_p,c} &= \mathrm{E}|b^6_{p,k}| \sum_{\ell} r^6_{p,\ell} + 18\mathrm{E}|b^2_{p,k}|\mathrm{E}|b^4_{p,k}| \sum_{j<\ell} r^4_{p,j} r^2_{p,\ell} + 36[\mathrm{E}|b^2_{p,k}|]^3 \sum_{i<j<\ell} r^2_{p,i} r^2_{p,j} r^2_{p,\ell} \\
\chi_{j_p,nc,1} &= \mathrm{E}(b^6_{p,k}) \sum_{\ell} r^6_{p,\ell} \\
\chi_{j_p,nc,2} &= \mathrm{E}(b^4_{p,k}|b^2_{p,k}|) \sum_{\ell} r^6_{p,\ell} + 10\mathrm{E}(b^4_{p,k})\mathrm{E}|b^2_{p,k}| \sum_{j<\ell} r^4_{p,j} r^2_{p,\ell} \\
\chi_{j_p,nc,3} &= \mathrm{E}(b^2_{p,k}|b^4_{p,k}|) \sum_{\ell} r^6_{p,\ell} + 16\mathrm{E}(b^4_{p,k})\mathrm{E}|b^2_{p,k}| \sum_{j<\ell} r^4_{p,j} r^2_{p,\ell}.
\end{aligned} \tag{11}$$

In the second case, $j_p(t)$ is assumed to be zero-mean stationary and Gaussian. It is then straightforward to prove, from SO, FO and SIO cumulant expressions [33], that the FO statistics of $j'_{p,k}$ are given by

$$\kappa_{j_p,c} = 2 + |\gamma_{j_p}|^2, \;\; \kappa_{j_p,nc,1} = 3\gamma^2_{j_p} \;\text{ and }\; \kappa_{j_p,nc,2} = 3\gamma_{j_p}, \tag{12}$$

whereas the SIO statistics are given by

$$\chi_{j_p,c} = 3(2 + 3|\gamma_{j_p}|^2), \;\; \chi_{j_p,nc,1} = 15\gamma^3_{j_p}, \;\; \chi_{j_p,nc,2} = 15\gamma^2_{j_p} \;\text{ and }\; \chi_{j_p,nc,3} = 3\gamma_{j_p}(4 + |\gamma_{j_p}|^2). \tag{13}$$

Finally, in the third case, $j_p(t)$ are impulsive CCI, where $j_{p,k} = \rho_{p,k} e^{i\theta_{p,k}}$ where $\rho_{p,k}$ and $\theta_{p,k}$ are independent random variables. $\rho_{p,k}$ is Bernoulli distributed, taking amplitude μ with probability q and 0 with probability $1-q$, and $\theta_{p,k}$ is uniformly distributed either on $[0, 2\pi]$, or drawn from the set of two values $\{0, \pi\}$. In the first case, $j_{p,k}$ is circular at any order, whereas in the second case $j_{p,k}$ is rectilinear. In both cases, we obtain:

$$\kappa_{j_p,c} = \frac{1}{q} \;\text{ and }\; \chi_{j_p,c} = \frac{1}{q^2}, \tag{14}$$

whereas in the second case, we obtain

$$\kappa_{j_p,nc,1} = \frac{1}{q}, \;\; \kappa_{j_p,nc,2} = \frac{1}{q}, \;\; \chi_{j_p,nc,1} = \frac{1}{q^2}, \;\; \chi_{j_p,nc,2} = \frac{1}{q^2} \;\text{ and }\; \chi_{j_p,nc,3} = \frac{1}{q^2}. \tag{15}$$

2.3. Problem formulation

The problem addressed in this paper is to detect the symbols a_k from the observations $\mathbf{x}_k$ through an MMSE approach. Naturally, the best estimate y_k of a_k according to the MMSE criterion is the conditional expectation $y_k = \mathrm{E}(a_k|\mathbf{x}_k)$. Note that for respectively circular or non-circular mutually Gaussian distributions of $(a_k, \mathbf{x}_k)$, this conditional expectation becomes linear or widely linear [5]. But for non-Gaussian distribution of $(a_k, \mathbf{x}_k)$, the derivation of this conditional expectation becomes generally non-linear in $\mathbf{x}_k$ and needs this distribution, which is unknown in practice. For this reason, we consider in this paper an approximation of this conditional expectation through the analysis of a particular class of non-linear filters corresponding to the complex Volterra (CV) filters, introduced for the first time in [11] and [12] in the context of detection and estimation. The general model of a memoryless full Mth-order time invariant CV filter is defined by

$$y_k = \sum_{m=0}^{M} \sum_{q=0}^{m} \mathbf{w}^H_{m,q} (\mathbf{x}_k^{\oslash(m-q)} \otimes \mathbf{x}_k^{*\oslash q}). \tag{16}$$

Assuming $\mathbf{w}_{0,0} = \mathbf{0}$, (16) defines a WL filter [5] for $M = 1$ and a full complex linear-quadratic filter [22] for $M = 2$. (16) can be compactly written in the form

$$y_k = \widetilde{\mathbf{w}}^H \widetilde{\mathbf{x}}_k, \tag{17}$$

where $\widetilde{\mathbf{w}} \overset{\text{def}}{=} (\mathbf{w}^T_{0,0}, \mathbf{w}^T_{1,0}, \mathbf{w}^T_{1,1}, \mathbf{w}^T_{2,0}, \mathbf{w}^T_{2,1}, \mathbf{w}^T_{2,2}, ..., \mathbf{w}^T_{M,M})^T$ and $\widetilde{\mathbf{x}}_k \overset{\text{def}}{=} (1, \mathbf{x}^T_k, \mathbf{x}^H_k, \mathbf{x}^T_k \oslash \mathbf{x}^T_k, \mathbf{x}^T_k \otimes \mathbf{x}^H_k, \mathbf{x}^H_k \oslash \mathbf{x}^H_k, ..., \mathbf{x}_k^{*\oslash M})^T$ is the non-redundant augmented observation. The problem of the optimal Mth-order CV filter is then to find $\widetilde{\mathbf{w}}$ minimizing the MSE between y_k and a_k.

3. Third-order complex Volterra MMSE receiver

3.1. Mth-order complex Volterra MMSE filter

The full Mth-order CV MMSE filter corresponds to the filter $\widetilde{\mathbf{w}}$ which minimizes the criterion $\mathrm{MSE}(\widetilde{\mathbf{w}}) = \mathrm{E}|a_k - \widetilde{\mathbf{w}}^H\widetilde{\mathbf{x}}_k|^2$. For stationary second-order signals $(a_k, \widetilde{\mathbf{x}}_k)$, this filter is classically given by

$$\widetilde{\mathbf{w}}_{\mathrm{CV-MMSE}} = \mathbf{R}_{\tilde{x}}^{-1}\mathbf{r}_{\tilde{x},a}, \tag{18}$$

with $\mathbf{R}_{\tilde{x}} \overset{\text{def}}{=} \mathrm{E}(\widetilde{\mathbf{x}}_k\widetilde{\mathbf{x}}_k^H)$ and $\mathbf{r}_{\tilde{x},a} \overset{\text{def}}{=} \mathrm{E}(\widetilde{\mathbf{x}}_k a_k^*)$. Note that in the case of linear and WL MMSE filters [31], for which $\mathbf{w}_{0,0}$ and 1 have been removed from $\widetilde{\mathbf{w}}$ and $\widetilde{\mathbf{x}}_k$, respectively, (18) reduces respectively to

$$\widetilde{\mathbf{w}}_{\mathrm{L-MMSE}} = \mathbf{R}_x^{-1}\mathbf{r}_{x,a} \text{ and } \widetilde{\mathbf{w}}_{\mathrm{WL-MMSE}} = \mathbf{R}_{\tilde{x}}^{-1}\mathbf{r}_{\tilde{x},a}, \tag{19}$$

where $\mathbf{R}_x \overset{\text{def}}{=} \mathrm{E}(\mathbf{x}_k\mathbf{x}_k^H)$ and $\mathbf{r}_{x,a} \overset{\text{def}}{=} \mathrm{E}(\mathbf{x}_k a_k^*)$, $\mathbf{R}_{\tilde{x}} \overset{\text{def}}{=} \mathrm{E}(\bar{\mathbf{x}}_k\bar{\mathbf{x}}_k^H)$ and $\mathbf{r}_{\bar{x},a} \overset{\text{def}}{=} \mathrm{E}(\bar{\mathbf{x}}_k a_k^*)$ with $\bar{\mathbf{x}}_k = [\mathbf{x}_k^T, \mathbf{x}_k^H]^T$, and where

$$\mathbf{r}_{x,a} = \mu_{s,a}\mathbf{h}_s \text{ and } \mathbf{r}_{\bar{x},a} = \mu_{s,a}\tilde{\mathbf{h}}_{s,\gamma},$$

with $\mu_{s,a} \overset{\text{def}}{=} \mu_s\pi_a r(0)$ and $\tilde{\mathbf{h}}_{s,\gamma} \overset{\text{def}}{=} [\mathbf{h}_s^T, \gamma_a^*\mathbf{h}_s^H]^T$ where $\gamma_a \overset{\text{def}}{=} \mathrm{E}(a_k^2)/\mathrm{E}|a_k^2|$ is the SO non-circular coefficient of the SOI symbol. However, in the general case, we obtain:

$$\mathbf{r}_{\tilde{x},a} = \mu_{s,a}\widetilde{\mathbf{h}}_{s,n}, \tag{20}$$

where the first two vectorial components of $\widetilde{\mathbf{h}}_{s,n}$ are $\mathbf{h}_s$ and $\gamma_a^*\mathbf{h}_s^*$, but the others depend on $\mathbf{h}_s$ and the statistics of both a_k and $\mathbf{n}_k$ of orders less or equal to M. This vector $\widetilde{\mathbf{h}}_{s,n}$ plays the role of an extended steering vector and $\widetilde{\mathbf{w}}_{\mathrm{CV-MMSE}}$ is also written in the form

$$\widetilde{\mathbf{w}}_{\mathrm{VC-MMSE}} = \mu_{s,a}\mathbf{R}_{\tilde{x}}^{-1}\widetilde{\mathbf{h}}_{s,n}. \tag{21}$$

The MSE obtained with the full Mth-order CV MMSE filter (18) is given by

$$\mathrm{MMSE} \overset{\text{def}}{=} \mathrm{MSE}[\widetilde{\mathbf{w}}_{\mathrm{CV-MMSE}}] = \pi_a - \mathbf{r}_{\tilde{x},a}^H\mathbf{R}_{\tilde{x}}^{-1}\mathbf{r}_{\tilde{x},a}. \tag{22}$$

If some components of the full Mth-order CV MMSE filter (16) are withdrawn, we obtain partial Mth-order CV MMSE filters. The increase $\Delta_{\mathrm{CV-MMSE}}$ of MMSE obtained by such partial Mth-order CV filters can be derived by partitioning $\widetilde{\mathbf{x}}_k$ into the retained, $\widetilde{\mathbf{x}}_{1,k}$ and the discarded, $\widetilde{\mathbf{x}}_{2,k}$ parts. Applying the matrix inversion lemma to the partitioned augmented covariance matrix $\mathbf{R}_{\tilde{x}}$ written as

$$\mathbf{R}_{\tilde{x}} = \begin{bmatrix} \mathbf{R}_{\tilde{x}_1} & \mathbf{R}_{\tilde{x}_{12}} \\ \mathbf{R}_{\tilde{x}_{12}}^H & \mathbf{R}_{\tilde{x}_{22}} \end{bmatrix},$$

where $\mathbf{R}_{\tilde{x}_{ij}} \overset{\text{def}}{=} \mathrm{E}(\widetilde{\mathbf{x}}_{i,k}\widetilde{\mathbf{x}}_{j,k}^H)$, $i, j = 1, 2$, the increase of MMSE given by the partial Mth-order CV MMSE filter that only uses $\widetilde{\mathbf{x}}_{1,k}$ is given by

$$\Delta_{\mathrm{CV-MMSE}} = (\mathbf{r}_{\tilde{x}_2,a}^H - \mathbf{r}_{\tilde{x}_1,a}^H\mathbf{R}_{\tilde{x}_{11}}^{-1}\mathbf{R}_{\tilde{x}_{12}})\left(\mathbf{R}_{\tilde{x}_{22}} - \mathbf{R}_{\tilde{x}_{12}}^H\mathbf{R}_{\tilde{x}_{11}}^{-1}\mathbf{R}_{\tilde{x}_{12}}\right)^{-1}(\mathbf{r}_{\tilde{x}_2,a} - \mathbf{R}_{\tilde{x}_{12}}^H\mathbf{R}_{\tilde{x}_{11}}^{-1}\mathbf{r}_{\tilde{x}_1,a}) \geq 0, \tag{23}$$

where $\mathbf{r}_{\tilde{x}_i,a} \overset{\text{def}}{=} \mathrm{E}(\widetilde{\mathbf{x}}_{i,k}a_k^*)$, $i, j = 1, 2$. Consequently, the term $\widetilde{\mathbf{x}}_{2,k}$ does not bring any information ($\Delta_{\mathrm{CV-MMSE}} = 0$) if in particular, it is not correlated with both a_k and $\widetilde{\mathbf{x}}_{1,k}$. An example of such a situation, in the presence of zero-mean signals with symmetric distributions, is the case where $\widetilde{\mathbf{x}}_{1,k}$ and $\widetilde{\mathbf{x}}_{2,k}$ gather the odd and even terms m of (16), respectively. Consequently, only Mth-order CV MMSE filters such that M is odd containing only polynomial terms of odd order m ought to be used. For such filters, $\widetilde{\mathbf{w}}$ and $\widetilde{\mathbf{x}}_k$ are reduced to $\widetilde{\mathbf{w}} = (\mathbf{w}_{1,0}^T, \mathbf{w}_{1,1}^T, \mathbf{w}_{3,0}^T, \mathbf{w}_{3,1}^T, \mathbf{w}_{3,2}^T, \mathbf{w}_{3,3}^T..., \mathbf{w}_{M,M}^T)^T$ and $\widetilde{\mathbf{x}}_k = (\mathbf{x}_k^T, \mathbf{x}_k^H, (\mathbf{x}_k^{\varnothing 3})^T, (\mathbf{x}_k^{\varnothing 2})^T \otimes \mathbf{x}_k^H, \mathbf{x}_k^T \otimes (\mathbf{x}_k^{\varnothing 2})^H, (\mathbf{x}_k^{\varnothing 3})^H..., (\mathbf{x}_k^{\varnothing M})^H)^T$. In this case, the components of $\widetilde{\mathbf{x}}_k$ can be rearranged in order as $\widetilde{\mathbf{x}}_k = [\mathbf{x}_k'^T, \mathbf{x}_k'^H]^T$ where $\mathbf{x}_k' = (\mathbf{x}_k^T, (\mathbf{x}_k^{\varnothing 3})^T, (\mathbf{x}_k^{\varnothing 2})^T \otimes \mathbf{x}_k^H, .., (\mathbf{x}_k^{\varnothing(M+1)/2})^T \otimes (\mathbf{x}_k^{\varnothing(M-1)/2})^H]^T$. Then, the partial Mth-order CV MMSE estimate y_k of a_k can be interpreted as the WL-MMSE estimate of a_k given $\mathbf{x}_k'$ and thus the partial Mth-order CV MMSE estimate inherits the properties of the WL-MMSE estimator [5].

In particular, for real-valued SOI symbols a_k, the estimate y_k given by the full Mth order CV MMSE filter (17) is real-valued. This property extends to any partial CV MMSE filter if $\widetilde{\mathbf{x}}_k$ contains the same terms as $\widetilde{\mathbf{x}}_k^*$. For partial CV MMSE structures that do not satisfy this condition, the estimate y_k of real-valued SOI symbols is complex-valued and the simple post processing consisting to take the real part z_k of y_k allows us to reduce the MMSE (22) because $|a_k - \mathrm{Re}(y_k)| \leq |a_k - y_k|$. Using (18) associated with such partial CV MMSE filters, we straightforwardly get:

$$\begin{aligned}\mathrm{MSE}_z &\overset{\text{def}}{=} \mathrm{E}\left(a_k - \mathrm{Re}(\widetilde{\mathbf{w}}_{\mathrm{CV-MMSE}}^H\widetilde{\mathbf{x}}_k)\right)^2 \\ &= \pi_a - \frac{3}{2}\mathbf{r}_{\tilde{x},a}^H\mathbf{R}_{\tilde{x}}^{-1}\mathbf{r}_{\tilde{x},a} + \frac{1}{2}\mathrm{Re}\left(\mathbf{r}_{\tilde{x},a}^H\mathbf{R}_{\tilde{x}}^{-1}\mathbf{C}_{\tilde{x}}\mathbf{R}_{\tilde{x}}^{-T}\mathbf{r}_{\tilde{x},a}^*\right) \leq \mathrm{MMSE},\end{aligned} \tag{24}$$

with $\mathbf{C}_{\tilde{x}} \overset{\text{def}}{=} \mathrm{E}(\widetilde{\mathbf{x}}_k\widetilde{\mathbf{x}}_k^T)$.

In contrast, if $\widetilde{\mathbf{x}}_{1,k}$ gathers the terms $(\mathbf{x}_k, \mathbf{x}_k^*)$ and $\widetilde{\mathbf{x}}_{2,k}$ the odd higher order terms, the terms $\widetilde{\mathbf{x}}_{2,k}$ are generally correlated with a_k and $\widetilde{\mathbf{x}}_{1,k}$ and thus contribute to decrease the MMSE with respect to that of the WL-MMSE filter. This proves the better performance, in terms of MMSE, of the partial Mth-order CV MMSE filter with only odd order terms with respect to the WL-MMSE filter.

Finally, note that in practice, $\mathbf{R}_{\tilde{x}}$ and $\mathbf{r}_{\tilde{x},a}$ are not known a priori and have to be estimated from a training sequence correlated with the SOI symbols and uncorrelated with the total noise, using a least square approach.

3.2. Orthogonal decomposition

To give an enlightening interpretation of a full or partial CV MMSE filter allowing one to understand its better behavior w.r.t. to the WL-MMSE filter, we extend the interpretation of the latter introduced in [30,31] using the orthogonal projection theorem. To this aim, we note that all the terms of $\widetilde{\mathbf{x}}_k$ contain a SOI component through the orthogonal decomposition deduced from the definition of $\mathbf{r}_{\tilde{x},a}$:

$$\widetilde{\mathbf{x}}_k = \left(\frac{\mathbf{r}_{\tilde{x},a}}{\pi_a}\right) a_k + \widetilde{\mathbf{i}}_k = \mu_s r(0)\widetilde{\mathbf{h}}_{s,n} a_k + \widetilde{\mathbf{i}}_k, \tag{25}$$

where a_k and $\widetilde{\mathbf{i}}_k$ are uncorrelated. From (25), the ratio of the powers of the SOI component and the associated global noise component at the output of an arbitrary CV filter $\widetilde{\mathbf{w}}$, defines an SINR at its output, given by:

$$\mathrm{SINR}(\widetilde{\mathbf{w}}) = \frac{|\widetilde{\mathbf{w}}^H \mathbf{r}_{\tilde{x},a}|^2}{\pi_a \widetilde{\mathbf{w}}^H \mathbf{R}_{\tilde{i}} \widetilde{\mathbf{w}}}, \tag{26}$$

where $\mathbf{R}_{\tilde{i}} \overset{\text{def}}{=} \mathrm{E}(\widetilde{\mathbf{i}}_k \widetilde{\mathbf{i}}_k^H)$ is the covariance matrix of the second component of $\widetilde{\mathbf{x}}_k$ (25) which gathers all its terms uncorrelated with the SOI symbol a_k. From (25) and (26), it is straightforward to deduce the following general relation linking the MSE and the SINR at the output y_k of an arbitrary CV filter $\widetilde{\mathbf{w}}$:

$$\mathrm{MSE}(\widetilde{\mathbf{w}}) = \pi_a \left| 1 - \frac{\widetilde{\mathbf{w}}^H \mathbf{r}_{\tilde{x},a}}{\pi_a} \right|^2 + \frac{|\widetilde{\mathbf{w}}^H \mathbf{r}_{\tilde{x},a}|^2}{\pi_a \mathrm{SINR}(\widetilde{\mathbf{w}})}. \tag{27}$$

We deduce from (27) that the CV filter $\widetilde{\mathbf{w}}$, which minimizes $\mathrm{MSE}(\widetilde{\mathbf{w}})$ under the constraint $\widetilde{\mathbf{w}}^H \mathbf{r}_{\tilde{x},a} = \pi_a$ is also the CV filter which maximizes $\mathrm{SINR}(\widetilde{\mathbf{w}})$ under the same constraint. This shows that under the constraint $\widetilde{\mathbf{w}}^H \mathbf{r}_{\tilde{x},a} = \pi_a$, MSE minimization and SINR maximization are equivalent criteria, which gives a physical interpretation of the SINR criterion (26) in term of MSE minimization. Without this constraint $\widetilde{\mathbf{w}}^H \mathbf{r}_{\tilde{x},a} = \pi_a$, (27) shows that the MSE minimization is no longer equivalent to SINR maximization, but $\widetilde{\mathbf{w}}_{\mathrm{CV-MMSE}}$, which minimizes $\mathrm{MSE}(\widetilde{\mathbf{w}})$ also maximizes $\mathrm{SINR}(\widetilde{\mathbf{w}})$. In this case it is no longer the only one.

It is easy to prove that the CV filters $\widetilde{\mathbf{w}}$ which maximize this SINR (26) are collinear to $\mathbf{R}_{\tilde{i}}^{-1}\mathbf{r}_{\tilde{x},a}$. Applying the matrix inversion lemma to $\mathbf{R}_{\tilde{i}} = \mathbf{R}_{\tilde{x}} - \pi_a^{-1}\mathbf{r}_{\tilde{x},a}\mathbf{r}_{\tilde{x},a}^H$ derived from the orthogonal decomposition (25), it is easy to verify that $\mathbf{R}_{\tilde{i}}^{-1}\mathbf{r}_{\tilde{x},a}$ and $\mathbf{R}_{\tilde{x}}^{-1}\mathbf{r}_{\tilde{x},a}$ are collinear. Consequently the CV filters $\widetilde{\mathbf{w}}$ which maximize the SINR (26) are collinear to $\widetilde{\mathbf{w}}_{\mathrm{CV-MMSE}}$ (18). The maximum of the SINR (26), denoted $\mathrm{SINR}_{\mathrm{CV-MMSE}}$ is thus given by:

$$\mathrm{SINR}_{\mathrm{CV-MMSE}} = \frac{1}{\pi_a}\mathbf{r}_{\tilde{x},a}^H \mathbf{R}_{\tilde{i}}^{-1}\mathbf{r}_{\tilde{x},a} = \frac{\pi_a^{-1}\mathbf{r}_{\tilde{x},a}^H \mathbf{R}_{\tilde{x}}^{-1}\mathbf{r}_{\tilde{x},a}}{1 - \pi_a^{-1}\mathbf{r}_{\tilde{x},a}^H \mathbf{R}_{\tilde{x}}^{-1}\mathbf{r}_{\tilde{x},a}}. \tag{28}$$

By applying the inversion matrix lemma to $\mathbf{R}_{\tilde{x}} = \pi_a^{-1}\mathbf{r}_{\tilde{x},a}\mathbf{r}_{\tilde{x},a}^H + \mathbf{R}_{\tilde{i}}$ in (22) and the constraint $\widetilde{\mathbf{w}}^H \mathbf{r}_{\tilde{x},a} = \pi_a$ in (27), we obtain using the first equality of (28):

$$\mathrm{MMSE} = \frac{\pi_a}{1 + \mathrm{SINR}_{\mathrm{CV-MMSE}}} \leq \frac{\pi_a}{\mathrm{SINR}_{\mathrm{CV-MMSE}}} = \mathrm{MSE}(\widetilde{\mathbf{w}}_{\mathrm{CV-MVDR}_2}), \tag{29}$$

where $\mathrm{MSE}(\widetilde{\mathbf{w}}_{\mathrm{CV-MVDR}_2})$ denotes the MSE at the output of the CV beamformer which minimizes $\widetilde{\mathbf{w}}^H \mathbf{R}_{\tilde{x}} \widetilde{\mathbf{w}}$ under the constraint $\widetilde{\mathbf{w}}^H \mathbf{r}_{\tilde{x},a} = \pi_a$. We see from (29) that $\mathrm{MSE}(\widetilde{\mathbf{w}}_{\mathrm{CV-MVDR}_2})$ approaches MMSE as $\mathrm{SINR}_{\mathrm{CV-MMSE}} \gg 1$.

Finally, we note that the different filters $\widetilde{\mathbf{w}}_{\mathrm{L-MMSE}}$ and $\widetilde{\mathbf{w}}_{\mathrm{WL-MMSE}}$ (19) studied in [2], $\widetilde{\mathbf{w}}_{\mathrm{L-MVDR}}$, $\widetilde{\mathbf{w}}_{\mathrm{WL-MVDR}_1}$ and $\widetilde{\mathbf{w}}_{\mathrm{WL-MVDR}_2}$ introduced respectively in [34], [35] and [31], and the CV beamformers $\widetilde{\mathbf{w}}_{\mathrm{CV-MVDR}_1}$ [25], $\widetilde{\mathbf{w}}_{\mathrm{CV-MVDR}_2}$ and $\widetilde{\mathbf{w}}_{\mathrm{CV-MMSE}}$ all minimize the output power $\widetilde{\mathbf{w}}^H \mathbf{R}_{\tilde{x}} \widetilde{\mathbf{w}}$ but under different constraints. Using the inclusion property of these constraints, we straightforwardly prove for both full and partial WL CV filters that generally

$$\mathrm{SINR}_{\mathrm{L-MVDR}} = \mathrm{SINR}_{\mathrm{L-MMSE}} \leq \mathrm{SINR}_{\mathrm{WL-MVDR}_1} \leq \mathrm{SINR}_{\mathrm{WL-MVDR}_2} = \mathrm{SINR}_{\mathrm{WL-MMSE}} \tag{30}$$

$$\mathrm{SINR}_{\mathrm{CV-MVDR}_1} \leq \mathrm{SINR}_{\mathrm{CV-MVDR}_2} = \mathrm{SINR}_{\mathrm{CV-MMSE}}. \tag{31}$$

Furthermore, using the inclusion principle in the minimization of the $\mathrm{MSE}(\widetilde{\mathbf{w}})$, we deduce:

$$\mathrm{SINR}_{\mathrm{L-MMSE}} \leq \mathrm{SINR}_{\mathrm{WL-MMSE}} \leq \mathrm{SINR}_{\mathrm{CV-MMSE}}. \tag{32}$$

But there is no generic relation between $\mathrm{SINR}_{\mathrm{WL-MVDR}_2} = \mathrm{SINR}_{\mathrm{WL-MMSE}}$ and $\mathrm{SINR}_{\mathrm{CV-MVDR}_1}$.

For partial CV MMSE filters for which the estimate y_k is complex-valued for real-valued a_k, the SINR (denoted SINR_z) associated with the MSE_z (24) obtained by taking the real part of y_k is no longer related to MSE_z by the relation (29). But simple algebraic manipulation allows us to prove the following expression:

$$\mathrm{SINR}_z = \frac{2\pi_a^{-1}\mathbf{r}_{\tilde{x},a}^H \mathbf{R}_{\tilde{x}}^{-1}\mathbf{r}_{\tilde{x},a}}{1 - 2\mathbf{r}_{\tilde{x},a}^H \mathbf{R}_{\tilde{x}}^{-1}\mathbf{r}_{\tilde{x},a} + \frac{\mathrm{Re}(\mathbf{r}_{\tilde{x},a}^H \mathbf{R}_{\tilde{x}}^{-1}\mathbf{C}_{\tilde{x}}\mathbf{R}_{\tilde{x}}^{-T}\mathbf{r}_{\tilde{x},a}^*)}{\mathbf{r}_{\tilde{x},a}^H \mathbf{R}_{\tilde{x}}^{-1}\mathbf{r}_{\tilde{x},a}}}. \tag{33}$$

Comparing (33) to (28), we see that

$$\mathrm{SINR}_z \geq \mathrm{SINR}_{\mathrm{CV-MMSE}} \tag{34}$$

because $\mathrm{MSE}_z \leq \mathrm{MMSE}$ implies from (24) that $\mathrm{Re}(\mathbf{r}_{\tilde{x},a}^H \mathbf{R}_{\tilde{x}}^{-1}\mathbf{C}_{\tilde{x}}\mathbf{R}_{\tilde{x}}^{-T}\mathbf{r}_{\tilde{x},a}^*) \leq \mathbf{r}_{\tilde{x},a}^H \mathbf{R}_{\tilde{x}}^{-1}\mathbf{r}_{\tilde{x},a}$.

3.3. Third-order complex Volterra MMSE filter

For reasons of implementation complexity, we only consider in the following Mth-order CV MMSE filters with $M = 3$ and odd order terms only (i.e. $m = 1, 3$), whose input/output relation is given by

$$y_k = \overbrace{\underbrace{\mathbf{w}_{1,0}^H \mathbf{x}_k}_{WL} + \mathbf{w}_{1,1}^H \mathbf{x}_k^*}^{L} + \underbrace{\mathbf{w}_{3,0}^H [\mathbf{x}_k \oslash \mathbf{x}_k \oslash \mathbf{x}_k]}_{C(0)} + \underbrace{\mathbf{w}_{3,1}^H [(\mathbf{x}_k \oslash \mathbf{x}_k) \otimes \mathbf{x}_k^*]}_{C(1)} + \underbrace{\mathbf{w}_{3,2}^H [\mathbf{x}_k \otimes (\mathbf{x}_k^* \oslash \mathbf{x}_k^*)]}_{C(2)} + \underbrace{\mathbf{w}_{3,3}^H [\mathbf{x}_k^* \oslash \mathbf{x}_k^* \oslash \mathbf{x}_k^*]}_{C(3)} \stackrel{\text{def}}{=} \widetilde{\mathbf{w}}^H \widetilde{\mathbf{x}}_k, \tag{35}$$

where $\widetilde{\mathbf{w}}$ is defined by (18), but where $\widetilde{\mathbf{w}}$ and $\widetilde{\mathbf{x}}_k$ are now restricted to $\widetilde{\mathbf{w}} = [\mathbf{w}_{1,0}^T, \mathbf{w}_{1,1}^T, \mathbf{w}_{3,0}^T, \mathbf{w}_{3,1}^T, \mathbf{w}_{3,2}^T, \mathbf{w}_{3,3}^T]^T$ and $\widetilde{\mathbf{x}}_k = [\mathbf{x}_k^T, \mathbf{x}_k^H, \mathbf{x}_k^{\oslash 3}, \mathbf{x}_k^{\oslash 2} \oslash \mathbf{x}_k^T, \mathbf{x}_k^T \oslash \mathbf{x}_k^{*\oslash 2}, \mathbf{x}_k^{*\oslash 3}]^T$, respectively. A filter defined by (35) is called a full WL cubic filter or a WL-C(0,1,2,3) filter, i.e., a WL-Cubic filter taking into account the cubic terms 0, 1, 2 and 3. We will see in Section 4 that partial linear or WL-Cubic MMSE filters with a single or double third-order term 0, 1, 2 or 3 in (35), called L-C(q_1), L-C(q_1, q_2), WL-C(q_1) ($q_i = 0, 1, 2$ or 3) allow us to obtain an MSE equal or close to the MMSE (22) of the full CV structure, depending on the statistics of the signals. If we denote by N_q, the number of components of the term $C(q)$, $q = 0, 1, 2, 3$, which are non-redundant, then it is easy to prove that $N_0 = N_3 = \frac{N(N+1)(N+2)}{6}$ and $N_1 = N_2 = \frac{N^2(N+1)}{2}$.

4. Performance in the presence of one interferer

We analyze in this section the performance of different CV MMSE receivers for the observed model (3) with a single interferer ($P = 1$):

$$\mathbf{x}_k = \sqrt{\pi_s} a_k' \mathbf{h}_s + \sqrt{\pi_j} j_k' \mathbf{h}_j + \mathbf{n}_k. \tag{36}$$

In particular, we compare the $\text{SINR}_{\text{CV-MMSE}}$ (28) to the SINR_{L} and SINR_{WL} given by the linear and WL MMSE beamformers (19), respectively.

4.1. SINR at the output of linear and WL receivers

In this scenario, the SINR at the output of the linear MMSE beamformer is straightforwardly given by

$$\text{SINR}_{\text{L}} = \epsilon_s \left(1 - \frac{\epsilon_j}{1 + \epsilon_j} |\alpha|^2\right), \tag{37}$$

where ϵ_s and ϵ_j are defined by $\epsilon_s \stackrel{\text{def}}{=} \|\mathbf{h}_s\|^2 \pi_s / \eta_2$ and $\epsilon_j \stackrel{\text{def}}{=} \|\mathbf{h}_j\|^2 \pi_j / \eta_2$, while SNR and INR denote the signal to noise ratio π_s/η_2 and the interference to noise ratio π_j/η_2 per antenna. α, such that $0 \leq |\alpha| \leq 1$, is the spatial correlation coefficient between the interference and the SOI, defined by

$$\alpha \stackrel{\text{def}}{=} |\alpha| e^{i\phi} \stackrel{\text{def}}{=} \mathbf{h}_s^H \mathbf{h}_j / \|\mathbf{h}_s\| \|\mathbf{h}_j\|. \tag{38}$$

We clearly see from (37) that SINR_{L} tends to zero for a strong CCI ($\epsilon_j \gg 1$) for $|\alpha| = 1$ and thus cannot perform SAIC.

For arbitrary rectilinear SOI and CCI signals, the SINR at the output of the WL MMSE beamformer is given [31] by:

$$\text{SINR}_{\text{WL}} = 2\epsilon_s \frac{1 + 2\epsilon_j - \epsilon_j |\alpha|^2 (1 + \cos(2\phi))}{1 + 2\epsilon_j} \tag{39}$$

and is approximated for strong CCI (i.e., for $\epsilon_j \gg 1$) [2] by:

$$\text{SINR}_{\text{WL}} \approx 2\epsilon_s \left(1 - |\alpha|^2 \cos^2 \phi\right). \tag{40}$$

Relation (40) shows that the WL-MMSE receiver performs SAIC (for which $|\alpha| = 1$) if $\phi \neq 0$ thanks to a phase diversity between the SOI and CCI, with decreasing performance as $|\phi|$ decreases to zero. Furthermore, we note that by averaging w.r.t. uniform ϕ, we get:

$$\overline{\text{SINR}}_{\text{WL}} \approx \epsilon_s \text{ for } |\alpha| = 1 \text{ and } \epsilon_j \gg 1. \tag{41}$$

4.2. Theoretical SINR at the output of CV receivers

In contrast to rels. (37) and (39), the derivation of the SINR at the output of the CV MMSE receivers is much more intricate. But using MATLAB symbolic algebra and calculus tools, we have proved that this output SINR follows the rational fraction form:

$$\text{SINR}_{\text{CV}} = \frac{a_D \pi_j^D + \ldots + a_1 \pi_j + a_0}{b_{D+1} \pi_j^{D+1} + \ldots + b_1 \pi_j + b_0}, \tag{42}$$

where D depends on the considered partial CV MMSE structure and the coefficients $a_0, .., a_D, b_0, .., b_{D+1}$ are functions of π_s, η_2, γ_s, γ_j $\kappa_{s,c}$, $\kappa_{j,c}$, $\kappa_{s,nc,i}, \kappa_{j,nc,i}$ for $i = 1, 2$, $\chi_{s,c}$, $\chi_{j,c}$, $\chi_{s,nc,i}, \chi_{j,nc,i}$ for $i = 1, 2, 3$, $|\alpha|$, ϕ, $\|\mathbf{h}_s\|^2$ and $\|\mathbf{h}_j\|^2$. To enlighten (42), we have to specify the statistics of the involved signals. SOI and interference, both rectilinear and SO circular are only considered in the following because of the space limitation.

4.2.1. Rectilinear signals

For real-valued a'_k and j'_k, $b_{D+1}=0$ and the coefficients $a_0,..,a_D,b_0,..,b_D$ depend only on π_s, η_2, $\kappa_s \overset{\text{def}}{=} \kappa_{s,c}=\kappa_{s,nc,i}$, $\kappa_j \overset{\text{def}}{=} \kappa_{j,c}=\kappa_{j,nc,i}$, $\chi_s \overset{\text{def}}{=} \chi_{s,c}=\chi_{s,nc,i}$, $\chi_j \overset{\text{def}}{=} \chi_{j,c}=\chi_{j,nc,i}$, $|\alpha|$ and ϕ. It is easy to prove by following decomposition (23), that discarding the WL or any cubic terms in (35) contribute to increase the MMSE and thus to decrease the SINR w.r.t. the full CV structure. This property will be illustrated in Subsection 4.3 where it is shown that the SINR of the partial WL-C(i) ($i=0,1,2$ or 3) MMSE receivers are nevertheless close of that of the full CV MMSE structure. For these structures, the maximum value of D in (42) is 4 and we have proved the following asymptotic results, for arbitrary N according to the values of $\chi_j-\kappa_j^2\geq 0$:

For $\chi_j-\kappa_j^2=0$, which occurs i.i.f. $j'_k=\pm 1/\sqrt{q}$ with probability $q>0$ and 0 with probability $1-q$ (see Appendix), we get:

$$\lim_{\pi_j\to\infty}\text{SINR}_{\text{WL-C}(i)}=\frac{a_3}{b_3}=2\epsilon_s,\ \text{for } i=0,1,2,3 \text{ and for all } \alpha=|\alpha|e^{i\phi}. \tag{43}$$

For $q=1$, this case corresponds to synchronized BPSK CCI ($\tau_j=0$) (see Appendix) for digital linearly modulated CCI (7) and for $0<q<1$, it corresponds to rectilinear Bernoulli distributed CCI for impulsive CCI.

For $\chi_j-\kappa_j^2>0$, i.e., for arbitrary rectilinear CCI, neither synchronized BPSK modulated, nor Bernoulli distributed:

$$\lim_{\pi_j\to\infty}\text{SINR}_{\text{WL-C}(i)}=\frac{a_4}{b_4}=2\epsilon_s\left(1-|\alpha|^2\cos^2\phi\right),\ \text{for } i=0,1,2,3. \tag{44}$$

Relation (43) shows that for synchronized BPSK CCI and rectilinear Bernoulli distributed CCI, the CCI is completely removed and the SAIC occurs, but without any SINR loss whatever the phase difference ϕ contrary to WL filters (40) for which a loss of $(1-|\alpha|\cos^2\phi)$ occurs. In this case, the performance gain with respect to the WL MMSE receiver (40) increases with $|\phi|$. This power's discrimination is generally strong in full-duplex systems [36]. For non-synchronized BPSK modulated CCI, despite the absence of gain brought by WL-C(i) MMSE receivers with respect to WL MMSE receivers for infinitely strong CCI, it is possible to show still significant gains in SINR for strong but not infinitely strong CCI as shown in Subsection 4.3.

Furthermore our MATLAB symbolic tools allow us to refine (43) for both $\epsilon_s\gg 1$ and $\epsilon_j\gg 1$ with $\epsilon_s/\epsilon_j\ll 1$, for which we get for $|\alpha|=1$:

$$\text{SINR}_{\text{WL-C}(0)}=\text{SINR}_{\text{WL-C}(3)}\approx 2\epsilon_s-\frac{\epsilon_s}{\epsilon_j}\left((20\epsilon_s+9)\cos(2\phi)+2\epsilon_s\cos(4\phi)+18\epsilon_s+9\right), \tag{45}$$

$$\text{SINR}_{\text{WL-C}(1)}=\text{SINR}_{\text{WL-C}(2)}\approx 2\epsilon_s-\frac{\epsilon_s}{\epsilon_j}\left((12\epsilon_s+3)\cos(2\phi)+2\epsilon_s\cos(4\phi)+10\epsilon_s+3\right), \tag{46}$$

which gives by averaging w.r.t. uniform ϕ

$$\overline{\text{SINR}}_{\text{WL-C}(0)}=\overline{\text{SINR}}_{\text{WL-C}(3)}\approx 2\epsilon_s-\frac{\epsilon_s}{\epsilon_j}\left(18\epsilon_s+9\right), \tag{47}$$

$$\overline{\text{SINR}}_{\text{WL-C}(1)}=\overline{\text{SINR}}_{\text{WL-C}(2)}\approx 2\epsilon_s-\frac{\epsilon_s}{\epsilon_j}\left(10\epsilon_s+3\right). \tag{48}$$

Consequently the partial structures WL-C(1) and WL-C(2) are preferred w.r.t. the partial structures WL-C(0) and WL-C(3). All these partial structures WL-C(i) naturally outperform the WL filter for which $\overline{\text{SINR}}_{\text{WL}}\approx\epsilon_s$ for $\epsilon_j\gg 1$ (41).

Finally, note that for $\phi=0$ and $|\alpha|=1$, for which $\text{SINR}_{\text{WL}}\sim\frac{\epsilon_s}{\epsilon_j}$ when $\epsilon_j\to\infty$ (39), we have proved that

$$\lim_{\pi_j\to\infty}\text{SINR}_{\text{WL-C}(i)}/\text{SINR}_{\text{WL}}=1+\frac{(3-\kappa_j)^2}{\chi_j-\kappa_j^2}. \tag{49}$$

There is naturally no gain for real-valued Gaussian distributed CCI for which $\kappa_j=3$ (see (12)) and an asymptotic infinite gain for synchronized BPSK modulated or rectilinear Bernoulli distributed CCI.

4.2.2. Second-order circular signals

We consider here only second-order circular a'_k and j'_k invariant with rotation of $\pi/2$, which correspond for example to M-PSK ($M>2$) or $4M^2$ QAM ($M>1$) symbols a_k and $b_{p,k}$ or to circular Bernouili distributed CCI, for which $\kappa_{s,nc,2}=\chi_{s,nc,1}=\chi_{s,nc,3}=\kappa_{j,nc,2}=\chi_{j,nc,1}=\chi_{j,nc,3}=0$, $\kappa_{s,nc,1}\neq 0$, $\chi_{s,nc,2}\neq 0$, $\kappa_{j,nc,1}\neq 0$ and $\chi_{j,nc,2}\neq 0$. For these signals, we straightforward prove using decomposition (23), that the conjugate, C(0) and C(2) terms in (35) do not contribute to decrease the MMSE, and thus the partial structure L-C(1,3) is optimal for the MMSE criterion.

For the structures L-C(1), L-C(3) and L-C(1-3), we have proved that $D=7$ in (42) and $b_8=0$ i.i.f. $\chi_{j,c}-\kappa_{j,c}^2=0$, which occurs i.i.f. $|j'_k|=1/\sqrt{q}$ with probability $q>0$ and 0 with probability $1-q$ (see Appendix). For $q=1$, this case corresponds to synchronized ($\tau_j=0$) M-PSK CCI with $M>1$ (e.g., QPSK) (see Appendix) for digital linearly modulated CCI (7) or to non-filtered constant modulus modulations, and for $0<q<1$, it corresponds to circular Bernoulli distributed CCI for impulsive CCI. We have proved in particular that for synchronized QPSK modulated SOI and CCI:

$$\lim_{\pi_j\to\infty}\text{SINR}_{\text{L-C}(1)}=\frac{a_7}{b_7}=\epsilon_s\left(\frac{(1-\frac{1}{2}|\alpha^2|)+(1-|\alpha^2|)\epsilon_s}{1+(1-\frac{1}{2}|\alpha^2|)\epsilon_s}\right), \tag{50}$$

$$\lim_{\pi_j\to\infty}\text{SINR}_{\text{L-C}(3)}=\frac{a_5}{b_5}=\epsilon_s\left(\frac{1+\epsilon_s(1-|\alpha^2|)}{1+\epsilon_s+|\alpha^2|(8\epsilon_s+9)}\right), \tag{51}$$

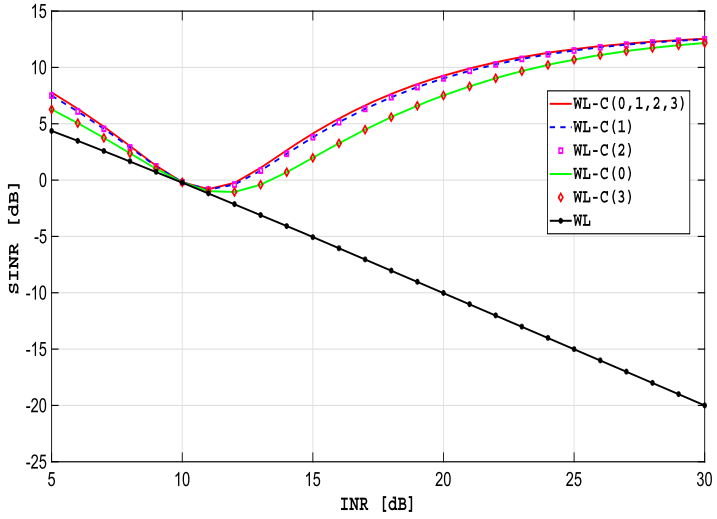

Fig. 1. SINR at the output of the WL-C(i) and WL-C(0,1,2,3) MMSE receivers as a function of the INR for $N = 1$, BPSK SOI and CCI with $\tau_j = 0$, $\phi = 0$ and SNR = 10 dB. (For interpretation of the colors in the figure(s), the reader is referred to the web version of this article.)

$$\lim_{\pi_j \to \infty} \mathrm{SINR}_{\mathrm{L-C}(1,3)} = \frac{a_7}{b_7} = \epsilon_s, \forall \alpha, \tag{52}$$

where (50) and (51) reduce for $|\alpha| = 1$ (including for $N = 1$) to

$$\lim_{\pi_j \to \infty} \mathrm{SINR}_{\mathrm{L-C}(1)} = \frac{a_3}{b_3} = \frac{\epsilon_s}{\epsilon_s + 2}, \forall \phi \tag{53}$$

$$\lim_{\pi_j \to \infty} \mathrm{SINR}_{\mathrm{L-C}(3)} = \frac{a_3}{b_3} = \frac{\epsilon_s}{9\epsilon_s + 10}, \forall \phi. \tag{54}$$

For $\chi_{j,c} - \kappa_{j,c}^2 > 0$, i.e., for either non-synchronized circular M-PSK CCI or non-filtered constant modulus modulations, we have for these structures $b_8 \neq 0$ in (42) and

$$\lim_{\pi_j \to \infty} \mathrm{SINR}_{\mathrm{L-C}(1)} = \lim_{\pi_j \to \infty} \mathrm{SINR}_{\mathrm{L-C}(1,3)} = \epsilon_s(1 - |\alpha^2|). \tag{55}$$

Relations (53) and (54) prove that the LC-(1) and LC-(3) MMSE receivers perform SAIC because $\mathrm{SINR}_{\mathrm{L-C}(1)}$ and $\mathrm{SINR}_{\mathrm{L-C}(3)}$ do not decrease to zero when $\pi_j \to \infty$. Relation (52) is the SINR given by the linear MMSE receiver without CCI (see (37)) which shows that for synchronized QPSK SOI and CCI, the CCI is completely removed at the output of L-C(1, 3) receiver whatever α (including for $N = 1$ for which $|\alpha| = 1$) thanks to a power's discrimination between the SOI and CCI. In this case, the performance gain with respect to the linear MMSE receiver (37) increases with ϵ_j. For non-synchronized QPSK modulated CCI, despite the absence of gain brought by the L-C(1, 3) MMSE receivers with respect to the linear MMSE receiver for infinitely strong CCI, it is possible to show still significant gains in SINR for strong but not infinitely strong CCI as shown in Subsection 4.3.

4.3. SINR performance illustrations

We start by focusing on the case of a single antenna to evaluate the enhancement of the SAIC given by third-order MMSE CV receivers. In all the illustrations, the SNR is fixed to $\epsilon_s = \pi_s/\eta_2 = 10$ dB. Fig. 1 compares the SINR at the output of the WL-C(i), $i = 0, 1, 2, 3$ and WL-C(0,1,2,3) receivers for BPSK SOI and CCI in the worst situation ($\tau_j = 0$, $\phi = 0$) as a function of the INR $= \pi_j/\eta_2 = \epsilon_j$. We see that the partial structures almost achieve the SINR of the full CV structure and the WL-C(1) and WL-C(2) structures are slightly better than the WL-C(0) and WL-C(3) structures (as predicted by (45), (46)) that outperform the WL filter.

As described in Subsection 3.2, there is a possible improvement of the partial WL-C(i), $i = 0, 1, 2, 3$ structures for BPSK SOI symbols by using a post processing consisting to take the real part z_k of CV MMSE receiver output. Fig. 2, confirms our theoretical analysis (34), but the modified structure WL-C(1) presents a small improvement w.r.t. the same partial structure based on y_k.

Figs. 3 and 4 show the SINR at the output of the WL-C(1) and WL receivers for BPSK SOI and CCI as a function of ϕ for different values of τ_j/T for a roll-off of 0.3, and as a function of τ_j/T for different values of the roll-off ω for $\phi = 0$, respectively. In the same way, Figs. 5 and 6 show the SINR at the output of the L-C(1, 3) and linear receivers for QPSK SOI and CCI. For all these figures, INR = $\epsilon_j = \pi_j/\eta_2 = 30$ dB. These four figures show still significant gain in SINR which decreases when the roll off ω of $v(t)$ decreases and $\tau_j \in [0, T/2]$ increases. This is explained by the presence of increasing inter-symbol interference due to the pulse shaping filter, which Gaussianizes the CCI component j'_k due to the central limit theorem and for which the gain strongly decreases. Furthermore, comparing Fig. 3 to 5, we see that the SINR at the output of the WL-C(1) receiver for BPSK SOI and CCI is sensitive to ϕ, in contrast to the SINR at the output of the L-C(1,3) receiver for QPSK SOI and CCI, which is not sensitive.

For the multiple antennas scenario, all performance behaviors of the CV MMSE receivers described in Figs. 2–6 are maintained with increasing SINR as $|\alpha|$ decreases and with an SINR enhancement due to spatial diversity because $\epsilon_s = \|\mathbf{h}_s\|^2 \pi_s/\eta_2$, except a significant increasing of SINR observed in the neighborhood of $\tau_j/T = 0.5$ w.r.t. Figs. 4 and 6.

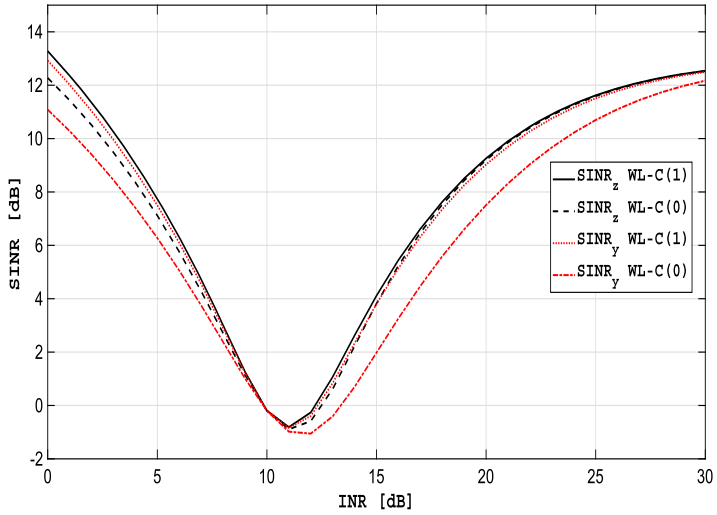

Fig. 2. SINR and SINR_z at the output of the WL-C(1) and WL-C(0) MMSE receivers as a function of the INR for $N = 1$, BPSK SOI and CCI with $\tau_j = 0$, $\phi = 0$ and SNR = 10 dB.

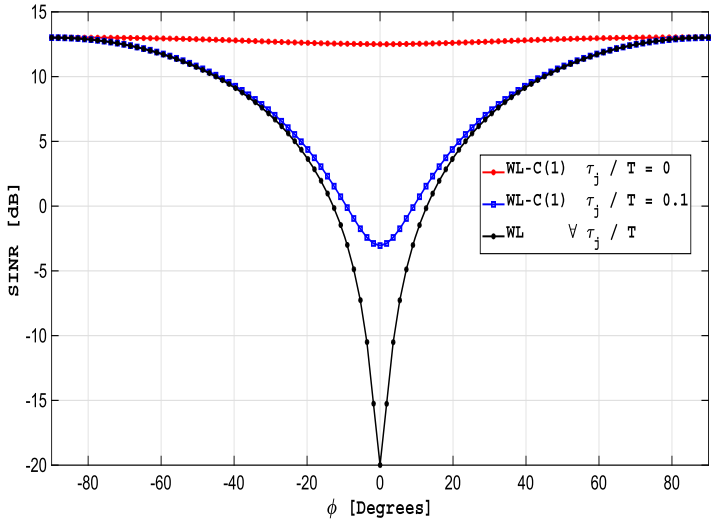

Fig. 3. $\text{SINR}_{\text{WL}-\text{C}(1)}$ and SINR_{WL} as a function of ϕ for BPSK SOI and CCI for $N = 1$, $\omega = 0.3$ and SNR = 10 dB.

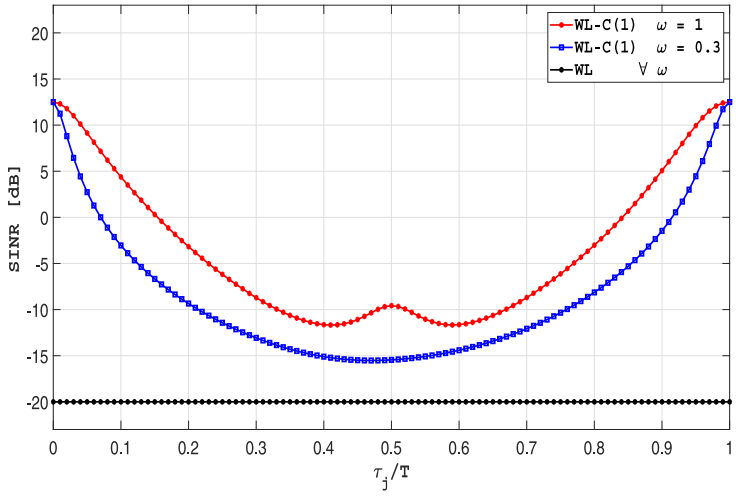

Fig. 4. $\text{SINR}_{\text{WL}-\text{C}(1)}$ and SINR_{WL} as a function of τ_j/T for BPSK SOI and CCI for $N = 1$, $\phi = 0$ and SNR = 10 dB.

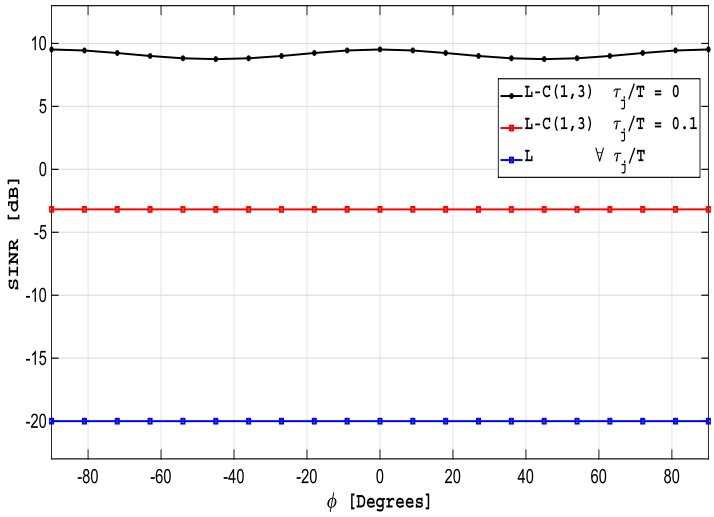

Fig. 5. $\text{SINR}_{\text{L-C(1,3)}}$ and SINR_{L} as a function of ϕ for QPSK SOI and CCI for $N = 1$ and SNR = 10 dB.

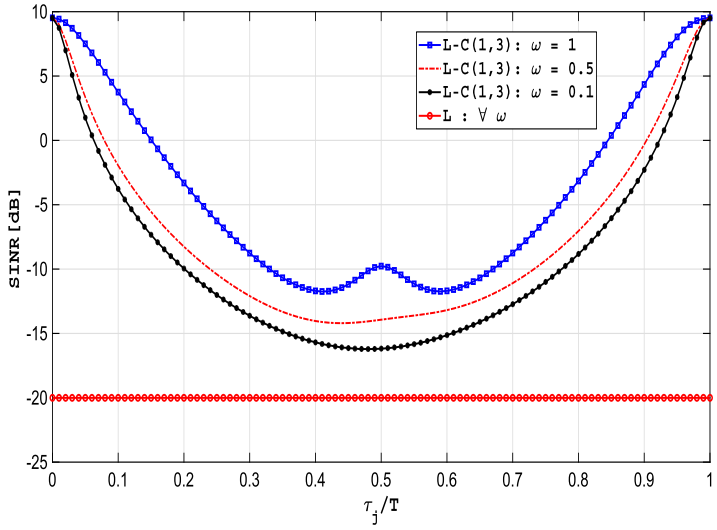

Fig. 6. $\text{SINR}_{\text{L-C(1,3)}}$ and SINR_{L} as a function of τ_j/T for QPSK SOI and CCI for $N = 1$, $\phi = 0$ and SNR = 10 dB.

We compare now in Fig. 7, the theoretical SINR at the output of the linear, WL and WL-C(1) MMSE beamformers against their equivalent MVDR_1 beamformers, which take into account the non-circularity and/or the non-Gaussiannity of the interference only (i.e., linear MVDR or Capon [34], WL MVDR_1 [35] and WL-C(1) MVDR_1 beamformers [25,37]) for $N = 2$, BPSK synchronized SOI and CCI symbols ($\tau_j = 0$) in the worst case $\phi = 0$, as a function of $|\alpha|$ for SNR $\pi_s/\eta_2 = 10$ dB, INR $\pi_s/\eta_2 = 30$ dB and a roll-off $\omega = 0.3$. Note that for the MVDR_1 beamformers, the comparison is shown with the time-averaged theoretical SINR because these beamformers have no knowledge of the SOI. This figure also shows the theoretical SINR at the output of the WL-C(1) MVDR_1 beamformer for a square pulse shaping filtering [25]. This figure confirms the inequalities (30)-(32). It illustrates that the exploitation of the non-circularity and/or the non-Gaussiannity of the SOI, in addition to that of the CCI allows one to improve the performance of the MMSE beamformers with respect to the associated MVDR_1 beamformers. We also see that the power's discrimination effect of the WL-C(1) MMSE beamformer makes it possible to maintain a strong SINR for a module of the spatial correlation close to 1, unlike the other beamformers.

4.4. Symbol error rate performance

To complete the SINR performance analysis, we present in this subsection the SER of the SOI symbols $a_k \in \mathcal{A}$ obtained by simple threshold detectors at the output y_k of different CV MMSE filters:

$$y_k = \widetilde{\mathbf{w}}^H \widetilde{\mathbf{x}}_k = \mu_s r(0)(\widetilde{\mathbf{w}}^H \widetilde{\mathbf{h}}_{s,n}) a_k + \widetilde{\mathbf{w}}^H \widetilde{\mathbf{i}}_k \overset{\text{def}}{=} \alpha_s a_k + \widetilde{\mathbf{w}}^H \widetilde{\mathbf{i}}_k, \tag{56}$$

deduced from (25). Using the ML[1] receiver under the false assumption of both circular Gaussian total noise $\widetilde{\mathbf{w}}^H \widetilde{\mathbf{i}}_k$ and independent symbol a_k and noise part $\widetilde{\mathbf{w}}^H \widetilde{\mathbf{i}}_k$, the detected SOI symbol is given by

[1] We note that the implementation of the CV MMSE beamformer before the ML detection, although suboptimal allows one to break free from the knowledge of the parameters π_s, π_j, η_2, $\mathbf{h}_s$ and $\mathbf{h}_j$.

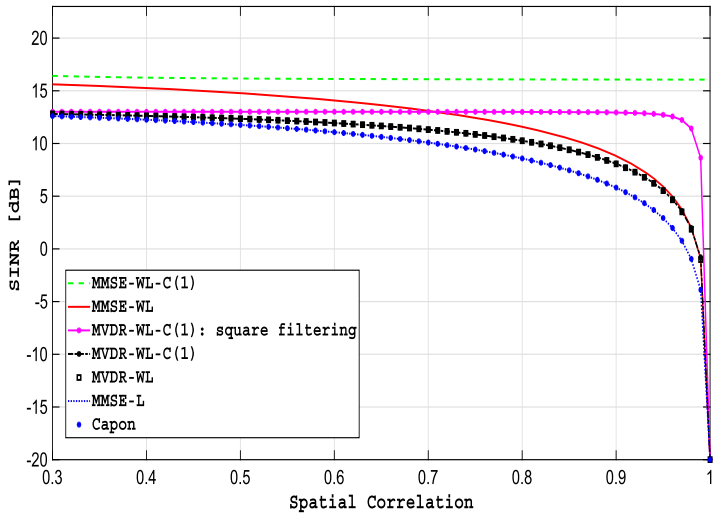

Fig. 7. SINR as function of $|\alpha|$ for different MVDR and MMSE beamformers for $N = 2$, BPSK SOI and CCI with $\tau_j = 0$, $\phi = 0$, SNR = 10 dB and INR = 30 dB.

$$\widehat{a}_k = \underset{a\in\mathcal{A}}{\text{Arg min}}\, |y_k - \alpha_s a|. \tag{57}$$

The derivation of the theoretical SER of such detector is very intricate, because, the noise part is not Gaussian distributed and not independent (although uncorrelated) from the symbol. Furthermore, we note the approximation deduced from the central limit theorem is not justified although $\widetilde{\mathbf{w}}^H\widetilde{\mathbf{i}}_k$ is the sum of a large number of random variables, because the variance of these random variables can be of different orders of magnitude, depending on π_s, π_j and η_2.

Consequently, we can only deduce the SER by Monte Carlo experiments. These SER are then compared to those of the optimal ML or MAP detector which knows all the parameters π_s, π_j, η_2, $\mathbf{h}_s$ and $\mathbf{h}_j$, given for synchronized symbols ($\tau_j = 0$) by:

$$\hat{a}_k = \underset{a\in\mathcal{A}}{\text{Arg max}} \sum_{b\in\mathcal{A}} \exp\left(-\frac{||\mathbf{x}_k - a\sqrt{\pi_s}\mathbf{h}_s - b\sqrt{\pi_j}\mathbf{h}_j||^2}{\eta_2}\right). \tag{58}$$

These SER have also been compared to those of the joint detector given by:

$$\hat{a}_k = \text{Arg}_{a\in\mathcal{A}} \min_{(a,b)\in\mathcal{A}^2} ||\mathbf{x}_k - a\sqrt{\pi_s}\mathbf{h}_s - b\sqrt{\pi_j}\mathbf{h}_j||^2, \tag{59}$$

with very similar SER.

We illustrate these SER in Figs. 8 and 9 as a function of the INR for an SNR equal to 9 dB for a single antenna ($N = 1$) for respectively BPSK and QPSK synchronized SOI and CCI symbols ($\tau_j = 0$) in the worst condition $\phi = 0$.

In Fig. 8(a), the SER given at the output of the WL-C(1) and WL MMSE filters are compared to those of the MAP receiver. The SINR at the outputs of the WL-C(1) and WL MMSE filters are also plotted in Fig. 8(b). This figure illustrates the power's discrimination allowed by the WL-C(1) MMSE receiver, for which its output SINR and SER practically reach their maximum $2\epsilon_s = 2\pi_s/\eta_2$ and minimum respectively for INR $\gg$ SNR. For INR $\approx$ SNR, the SOI and CCI symbols constellations of the input signal x_k overlap, so the output SINR reaches its minimum where the SER is maximum. Note also a rebound in the SER for INR $\approx$ SNR + 6 dB which is explained by a geometric ambiguity in the constellation of the observation y_k with respect to the reference constellation of the SOI.

Fig. 9(a) shows the SER at the output of the L-C(1,3), L-C(1) and linear MMSE filters which are compared to those of the MAP receiver. Compared to the SINR exhibited in Fig. 9(b), these figures also exhibit the power's discrimination allowed by the L-C(1,3) MMSE receiver, for which its output SINR attains its minimum for INR $\approx$ SNR and its maximum ϵ_s for strong CCI where the SER is minimum. So the SER and SINR obtained by the different CV MMSE receivers have consistent behaviors. This reinforces the meaning of the SINR defined by the orthogonal decomposition (26). Furthermore, we note that although the MAP receiver outperforms the WL-C(1) and L-C(1,3) MMSE receivers, their SERs are very close for strong CCI.

5. Performance in the presence of two interferers

In the presence of two interferers, the derivation of the SINR is very complicated and exceeds the capabilities of our MATLAB symbolic and calculus tools, so we limit our analysis to orthogonal interferers for which $\mathbf{h}_{j_1}^H\mathbf{h}_{j_2} = 0$, for both rectilinear or SO circular CCI and SOI.

5.1. SINR at the output of linear and WL MMSE receivers

Under these assumptions, the SINR at the output of the linear MMSE beamformer is straightforwardly given by

$$\text{SINR}_\text{L} = \epsilon_s\left(1 - \frac{|\alpha_1|^2\epsilon_{j_1}}{1+\epsilon_{j_1}} - \frac{|\alpha_2|^2\epsilon_{j_2}}{1+\epsilon_{j_2}}\right), \tag{60}$$

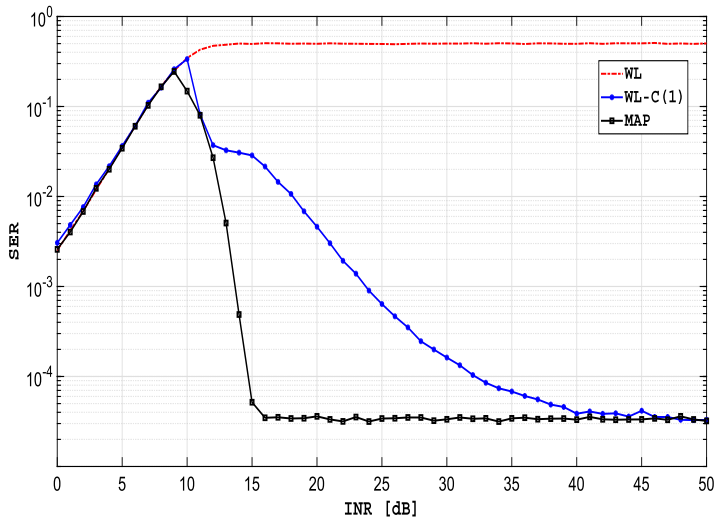

(a) SER

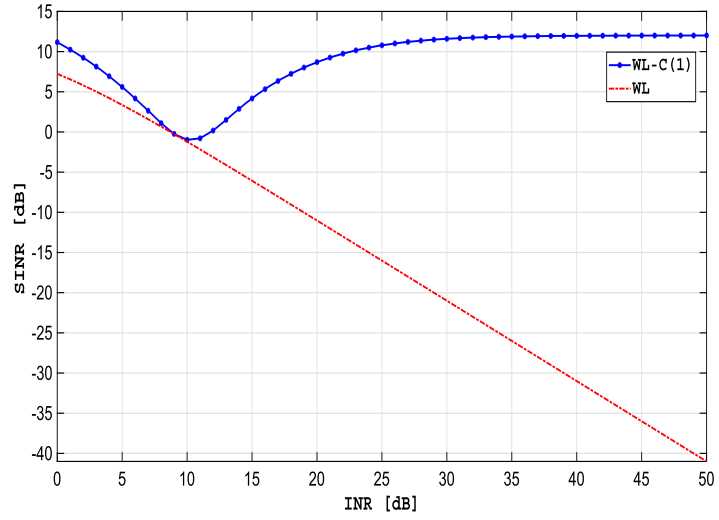

(b) SINR

Fig. 8. SER (a) and SINR (b) at the output of the WL, WL-C(1) MMSE and MAP receivers as a function of INR for $N = 1$, BPSK SOI and CCI with $\tau_j = 0$, $\phi = 0$ and SNR = 9 dB.

where $\epsilon_{j_i} \overset{\text{def}}{=} \|\mathbf{h}_{j_i}\|^2 \pi_{j_i}/\eta_2$ and $\alpha_i \overset{\text{def}}{=} |\alpha_i| e^{i\phi_i} = \mathbf{h}_s^H \mathbf{h}_{j_i}/\|\mathbf{h}_s\|\|\mathbf{h}_{j_i}\|$, $i = 1, 2$, whereas the SINR at the output of the WL MMSE beamformer is also straightforwardly given by

$$\text{SINR}_{\text{WL}} = 2\epsilon_s \left(1 - \frac{2|\alpha_1|^2 \cos^2(\phi_1)\epsilon_{j_1}}{1 + 2\epsilon_{j_1}} - \frac{2|\alpha_2|^2 \cos^2(\phi_2)\epsilon_{j_2}}{1 + 2\epsilon_{j_2}}\right), \tag{61}$$

for arbitrary rectilinear SOI and CCI. This SINR is approximated for strong CCI ($\epsilon_{j_1} \gg 1$ and $\epsilon_{j_2} \gg 1$) by

$$\text{SINR}_{\text{WL}} \approx 2\epsilon_s \left(1 - |\alpha_1|^2 \cos^2 \phi_1 - |\alpha_2|^2 \cos^2 \phi_2\right). \tag{62}$$

5.2. SINR and SER at the output of CV MMSE receivers

In the scenario of two orthogonal interferers, the derivation of the SINR at the output of CV MMSE receiver is very involved by our MATLAB's symbolic math toolbox. However, in the particular case of $N = 2$ for which $\|\mathbf{h}_s\|^2 = |\mathbf{h}_{j_1}\|^2 = |\mathbf{h}_{j_2}\|^2 = 2$, $|\alpha_1|^2 + |\alpha_2|^2 = 1$, with $\pi_{j_1} = \pi_{j_2} \overset{\text{def}}{=} \pi_j$ and $\phi_{j_1} = \phi_{j_2} \overset{\text{def}}{=} \phi_j$, $\tau_{j_1} = \tau_{j_2} = \tau_j = 0$, we have proved the following limits for BPSK SOI/CCI and QPSK SOI/CCI symbols, respectively:

$$\lim_{\pi_j \to \infty} \text{SINR}_{\text{WL}-\text{C}(1)} = \lim_{\pi_j \to \infty} \text{SINR}_{\text{WL}-\text{C}(0)} = 2\epsilon_s, \tag{63}$$

$$\lim_{\pi_j \to \infty} \text{SINR}_{\text{L}-\text{C}(1,3)} = \epsilon_s, \tag{64}$$

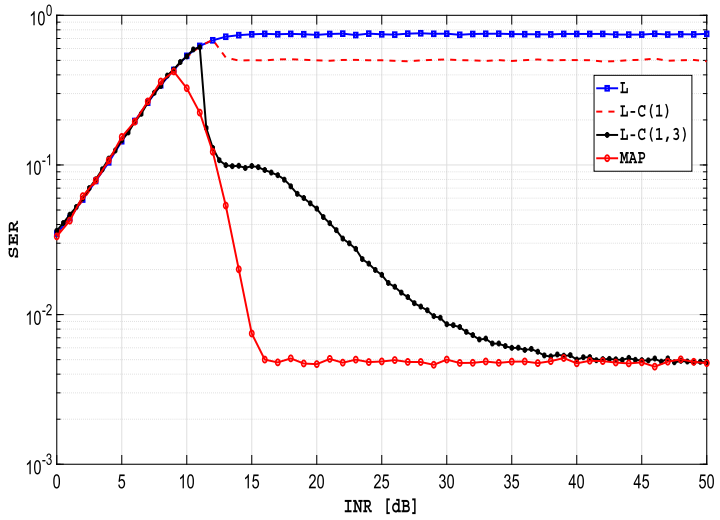

(a) SER

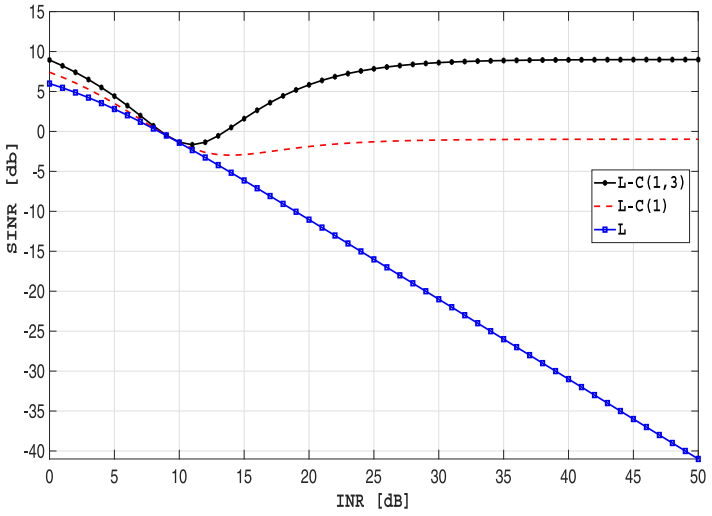

(b) SINR

Fig. 9. SER (a) and SINR (b) at the output of the Linear, LC(1), LC(1,3) MMSE and MAP receivers as a function of INR for $N = 1$, QPSK SOI and CCI with $\tau_j = 0$, $\phi = 0$ and SNR = 9 dB.

for all ϕ_j and α_1. These limiting values of SINR are those obtained for a single interference (see (43) for BPSK CCI and (52) for QPSK CCI). Both relations (63), (64) prove that these CV MMSE receivers completely remove the two interference terms with only $N = 2$ antennas thanks to a power's discrimination between the SOI and CCI.

To complete the SINR performance analysis, we present under the assumptions given in Section 4.4 with here SNR = 5 dB, a comparison of the behavior of the SINR and the SER at the output of the WL-C(1) and WL MMSE receivers with BPSK SOI and CCI as a function of the INR also defined by π_j/η_2. Similarly to Figs. 8 and 9, Fig. 10 illustrates the power's discrimination allowed by the WL-C(1) MMSE receiver, for which its output SINR reaches its minimum for two CCI when INR $\approx$ SNR and its maximum $2\epsilon_s = 4\pi_s/\eta_2$ for strong CCI where the SER is minimum. Note also the rebound in the SER for two CCI when INR $\approx$ SNR + 6 dB because of the ambiguity of the SOI constellation in x_k compared to those of the CCI.

6. Adaptive implementation

6.1. Presentation

In practical situations, the correlation matrix $\mathbf{R}_{\tilde{x}}$ and the intercorrelation vector $\mathbf{r}_{\tilde{x},a}$ are not known a priori, whereas a training sequence $(a_1, ..., a_K)$ uncorrelated with the interference is available after a synchronization process. Several adaptive implementations can be developed in this case. Assuming the observations $\mathbf{x}_k$ are stationary over blocks including K training symbols and L data symbols, we propose here to use an extension of the sample matrix inversion (SMI) algorithm [38] to implement (18). It consists to estimate the CV MMSE filter $\widetilde{\mathbf{w}}$ from K observations associated with the training sequence $(a_1, ..., a_K)$ by

$$\widehat{\widetilde{\mathbf{w}}} = \widehat{\mathbf{R}}_{\tilde{x}}^{-1} \widehat{\mathbf{r}}_{\tilde{x},a}, \tag{65}$$

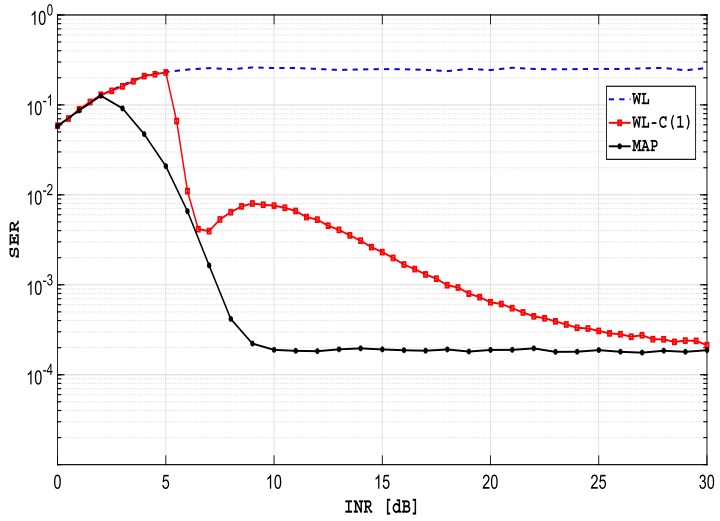

(a) SER

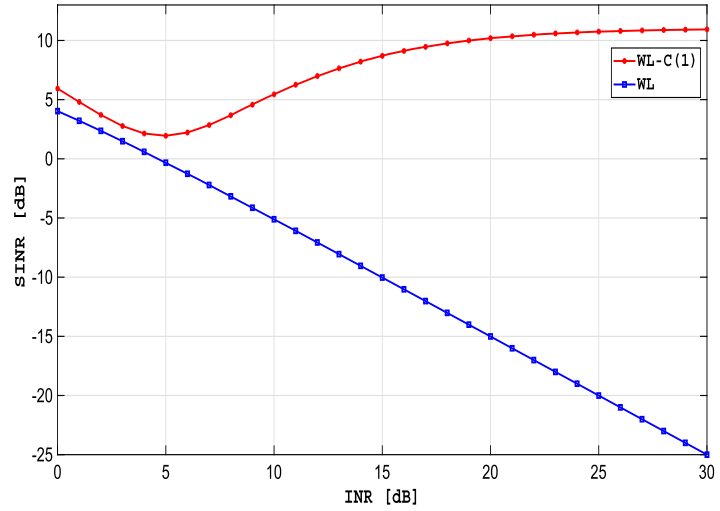

(b) SINR

Fig. 10. SER (a) and SINR (b) at the output of the WL, WL-C(1) MMSE receivers as a function of INR for $N = 2$, BPSK SOI, SNR = 5 dB and $P = 2$ orthogonal CCI with $\phi_j = 0$, $\tau_j = 0$ and $|\alpha_1| = \sqrt{2}/2$.

where $\widehat{\mathbf{R}}_{\tilde{x}}$ and $\widehat{\mathbf{r}}_{\tilde{x},a}$ are the empirical means $\frac{1}{K}\sum_{k=1}^{K}\tilde{\mathbf{x}}_k\tilde{\mathbf{x}}_k^H$ and $\frac{1}{K}\sum_{k=1}^{K}\tilde{\mathbf{x}}_k a_k^*$, respectively.

In this per block strategy of adaptation, the CV MMSE filter is estimated only on time per block of K training symbols and L data symbols (located for example on either side of the training symbols). To illustrate the role of K, we will consider the rate of convergence.

6.2. Rate of convergence

The rate of convergence of the SMI algorithm has been theoretically analyzed in many papers (see e.g. [38] for linear receivers). But the theoretical analysis of the CV SMI algorithm is beyond the scope of this paper and we simply illustrate its convergence through a Monte-Carlo experiment. For this purpose, we consider the case of BPSK synchronized SOI and CCI symbols ($\tau_j = 0$) in the worst condition $\phi = 0$ for $N = 2$, $P = 1$, SNR = 13 dB and INR = 33 dB. The SINR at the output of the third-order CV receiver implemented by the SMI algorithm from K observations is defined by:

$$\mathrm{SINR}(K) = \frac{|\widehat{\widetilde{\mathbf{w}}}^H \mathbf{r}_{\tilde{x},a}|^2}{\pi_a \widehat{\widetilde{\mathbf{w}}}^H \mathbf{R}_i \widehat{\widetilde{\mathbf{w}}}} = \frac{|\widehat{\widetilde{\mathbf{w}}}^H \mathbf{r}_{\tilde{x},a}|^2}{\pi_a \widehat{\widetilde{\mathbf{w}}}^H (\mathbf{R}_{\tilde{x}} - \pi_a^{-1}\mathbf{r}_{\tilde{x},a}\mathbf{r}_{\tilde{x},a}^H)\widehat{\widetilde{\mathbf{w}}}}. \tag{66}$$

Under these assumptions, Fig. 11 shows the variation, as a function of K, of the estimated mean value of $\mathrm{SINR}(K)$, $\widehat{\mathrm{E}}(\mathrm{SINR}(K))$ computed over 1000 runs, at the output of the WL-C(1) MMSE and WL-C(1) MVDR beamformers, compared to the WL MMSE and WL MVDR$_1$

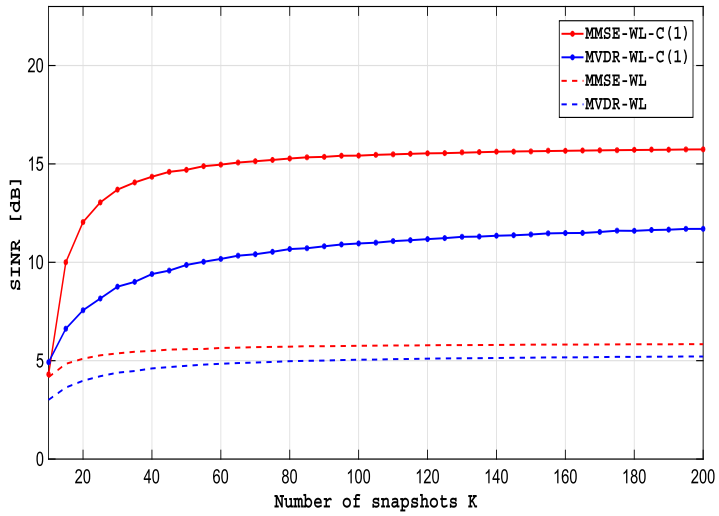

Fig. 11. $\widehat{\mathrm{E}}(\mathrm{SINR}(K))$ as a function of K for BPSK SOI and CCI, $N=2$, $P=1$ and $|\alpha|=0.95$, with $\tau_j=0$, $\phi=0$ and SNR = 10 dB.

beamformers. We verify that the steady state performances of the WL MVDR$_1$, WL MMSE and WL-C(1) MVDR$_1$ beamformers are upper bounded by the performance of the WL-C(1) MMSE beamformer, consistently with Fig. 7.

We see that in this scenario the necessary numbers of snapshots required to achieve optimal performance for high INR, are about 100 snapshots for the WL-C(1) MMSE and WL-C(1) MVDR$_1$ beamformers and 40 snapshots for the WL MMSE and WL MVDR$_1$ beamformers. Naturally the rate of convergence decreases for WL-C(1) beamformers w.r.t. WL ones because the number of entries is larger [38]. More precisely, the numbers of inputs of these receivers are $N_i=2N=4$ and $N_i=2N+N^2(N+1)/2=10$ for the WL MMSE and WL-C(1) MMSE beamformers, respectively, and the required number K of training symbols is roughly $K=10N_i$.

6.3. Complexity elements

We now give some complexity elements of some proposed third-order MMSE receivers compared to the linear and WL MMSE receivers. Denoting by N_i the number of input of these receivers, we get from the analysis presented at the end of Subsection 3.1:

- $N_i=N$ for a linear receiver,
- $N_i=2N$ for a WL receiver,
- $N_i=N+N^2(N+1)/2$ for a L-C(1) receiver,
- $N_i=N+N^2(N+1)/2+N(N+1)(N+2)/6$ for a L-C(1,3) receiver,
- $N_i=2N+N^2(N+1)/2$ for a WL-C(1) receiver,
- $N_i=2N+N^2(N+1)+N(N+1)(N+2)/3$ for a WL-C(0,1,2,3) receiver.

Assuming the adaptation is done from a per block strategy as explained in Subsection 6.1, the complexity of a receiver corresponds to the number of complex operations (comps) required to compute one estimated data symbol. Under these assumptions, the number of comps required to compute L receiver outputs from the L data symbols of a block, jointly with the associated complexity, are presented in the following:

$$\begin{aligned}
\widehat{\mathbf{R}}_{\widetilde{x}} &: N_i(N_i+1)(2K-1)/2 \text{ comps}\\
\widehat{\mathbf{r}}_{\widetilde{x},a} &: N_i(2K-1) \text{ comps}\\
\widehat{\mathbf{R}}_{\widetilde{x}}^{-1} &: 8N_i^3/3 \text{ comps}\\
\widehat{\widetilde{\mathbf{w}}}=\widehat{\mathbf{R}}_{\widetilde{x}}^{-1}\widehat{\mathbf{r}}_{\widetilde{x},a} &: N_i(2N_i-1) \text{ comps}\\
y_k=\widehat{\widetilde{\mathbf{w}}}^H\widetilde{\mathbf{x}}_k\ (1\le k\le K+L) &: (K+L)(2N_i-1) \text{ comps}\\
\text{overall number of operations} &: \frac{8N_i^3}{3}+\left(K+\frac{3}{2}\right)N_i^2+\left(5K+2L-\frac{5}{2}\right)N_i-K-L \text{ comps.}
\end{aligned}$$

In practical situations, K is often chosen as a multiple of N_i, which means that $K=\gamma N_i$, where γ is an integer such that $\gamma\ge 1$ to ensure the invertibility of the estimated correlation matrix of $\widetilde{\mathbf{x}}_k$. Otherwise, the number $\delta\overset{\text{def}}{=}L/K$ of data symbols per training symbol is of the order of a few units, depending on the stationarity of the observations. Under this assumption, the complexity (number of comps per data symbol) is given by

$$\text{Complexity} = \frac{1}{\delta}\left(1+\frac{8}{3\gamma}\right)N_i^2+\left(2+\frac{5}{\delta}+\frac{3}{2\delta\gamma}\right)N_i-\left(1+\frac{1}{\delta}+\frac{5}{2\delta\gamma}\right). \tag{67}$$

We deduce from these expressions that the complexity with respect to N is:

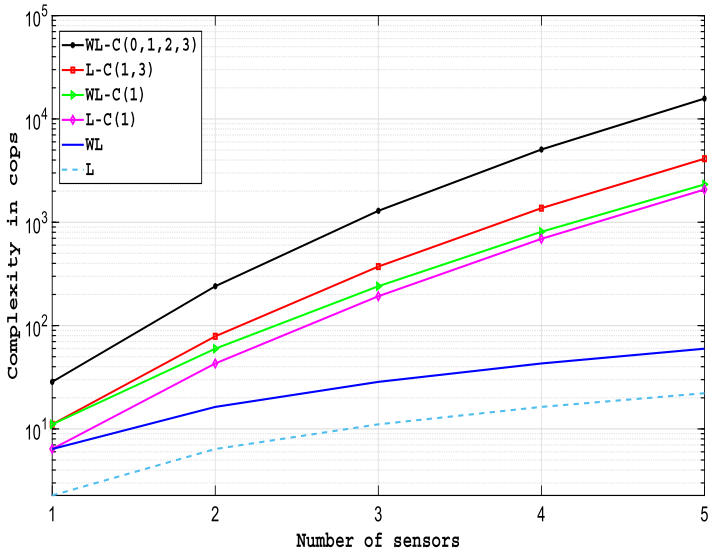

Fig. 12. Complexity of several first-order and third-order beamformers as a function of N, $\gamma = 20$, $\delta = 4$.

- $O(\delta^{-1}[1 + (8/3\gamma)]N^2)$ for a linear receiver,
- $O(\delta^{-1}[1 + (8/3\gamma)]4N^2)$ for a WL receiver,
- $O(\delta^{-1}[1 + (8/3\gamma)]N^6/4)$ for a L-C(1) receiver,
- $O(\delta^{-1}[1 + (8/3\gamma)]4N^6/9)$ for a L-C(1,3) receiver,
- $O(\delta^{-1}[1 + (8/3\gamma)]N^6/4)$ for a WL-C(1) receiver,
- $O(\delta^{-1}[1 + (8/3\gamma)]16N^6/9)$ for a WL-C(0,1,2,3) receiver.

To quantify the expressions of the complexity (67), Fig. 12 shows the variations of the complexity of several first and third-order MMSE receivers as a function of N for $\delta = 4$ and $\gamma = 20$. We note in particular from this figure, a very acceptable complexity of most of the proposed third-order MMSE receiver for small-scale systems ($1 \leq N \leq 5$) because the number of comps required by most of the receivers to generate an estimated data symbol does not exceed 500. Clearly large values of $\gamma = K/N_i$ and $\delta = L/K$ are of interest for the complexity point of view, whereas large values of γ improve the steady state performance of the estimated receiver and decrease the estimation variance of the latter. But γ and δ must be upper-bounded because the observations must be stationary over $K + L = \gamma(1 + \delta)N_i$ symbols. A tradeoff must therefore be found between (complexity and performance) and stationarity duration assumption.

7. Conclusion

Enlightening interpretations and related generic output SINR performance of the Mth-order CV MMSE receiver have been given in this paper using an orthogonal decomposition. A family of third-order CV MMSE receivers for the reception of digital linearly modulated SOI whose waveform is known corrupted by potentially non-Gaussian and non-circular interference has been introduced. Performances in term of SINR depending on the symbols constellation, the pulse shaping filter and relative phase and delays between the SOI and the CCI have been theoretically analyzed and comparisons w.r.t. output SER have been shown by Monte Carlo experiments. It has been proved that some of these receivers that exploit FO and SIO non-circularity of SOI and CCI, enhance WL receiver performance for SAIC of one rectilinear interference such as BPSK interference, whereas some other receivers allow us to fulfill SAIC of FO non-circular interference such as QPSK interference, by power's discrimination between SOI and CCI, result which is not possible from WL receivers. These results open new perspectives for enhanced SAIC in non-Gaussian and non-circular contexts, omnipresent in practice.

CRediT authorship contribution statement

All authors certify that they have participated sufficiently in the work to take public responsibility for the content, including participation in the concept, design, analysis, writing, or revision of the manuscript. Furthermore, each author certifies that this material or similar material has not been and will not be submitted to or published in any other publication.

Declaration of competing interest

The authors declare that they have no known competing financial interests or personal relationships that could have appeared to influence the work reported in this paper.

Appendix

Proof of condition of $\chi_j - \kappa_j^2 = 0$ in Subsection 4.2

Applying the Cauchy–Schwarz inequality to the random variables $|j_k'^3|$ and $|j_k'|$, we get: $[\mathrm{E}|j_k'^4|]^2 \leq \mathrm{E}|j_k'^6|\mathrm{E}|j_k'^2|$. Thus $\chi_j - \kappa_j^2 \geq 0$ with equality if and only if $|j_k'^3|$ and $|j_k'|$ are proportional, i.i.f. and $|j_k'|(|j_k'^2| - c) = 0$ with c constant, i.i.f. $j_k' = 0$ or $|j_k'^2| = c$. With $\mathrm{E}|j_k'^2| = 1$,

this is equivalent to $|j'_k| = 1/\sqrt{p}$ with probability p and 0 with probability $1-p$. For $p=1$, this is equivalent to $j'_k = \pm 1$ and $|j'_k| = 1$ for real-valued and second-order circular CCI, respectively. For digital modulated CCI, for which $j'_k = \frac{\sum_\ell b_\ell r((k-\ell)T-\tau_j)}{\sqrt{\sum_\ell b_\ell r((k-\ell)T-\tau_j)}}$, this corresponds to $r(iT-\tau_j)=0$, except for a value i_0 of i and because $r(t)$ is a Nyquist pulse $i_0 = 0$ and $\tau_j = 0$. □

References

[1] M. Bavand, S.D. Blostein, User selection and multiuser widely linear precoding for one-dimensional signalling, IEEE Trans. Veh. Technol. 67 (12) (Dec. 2018) 11642–11653.
[2] P. Chevalier, F. Pipon, New insights into optimal widely linear array receivers for the demodulation of BPSK, MSK and GMSK signals corrupted by noncircular interferences – application to SAIC, IEEE Trans. Signal Process. 54 (3) (March 2006) 870–883.
[3] H. Trigui, D.T.M. Slock, Performance bounds for cochannel interference cancellation within the current GSM standard, Signal Process. 80 (2000) 1335–1346.
[4] R. Meyer, W.H. Gerstacker, R. Schober, J.B. Huber, A single antenna interference cancellation algorithm for increased GSM capacity, IEEE Trans. Wirel. Commun. 5 (7) (July 2006) 1616–1621.
[5] B. Picinbono, P. Chevalier, Widely linear estimation with complex data, IEEE Trans. Signal Process. 43 (8) (Aug. 1995) 2030–2033.
[6] P.O. Amblard, M. Gaeta, J.L. Lacume, Statistics for complex variables and signals – part I and II, Signal Process. 53 (1) (Aug. 1996) 1–25.
[7] M.S. Arulampalam, S. Maskell, N. Gordon, T. Clapp, A tutorial on particle filters for online nonlinear/non-Gaussian Bayesian tracking, IEEE Trans. Signal Process. 50 (2) (Feb. 2002) 174–188.
[8] P.M. Djuric, J.H. Kotecha, J. Zhang, Y. Huang, T. Ghirmai, M.F. Bugallo, J. Miguez, Particle filtering, IEEE Signal Process. Mag. 20 (5) (2003) 19–38.
[9] L.M. Garth, H.V. Poor, Narrowband interference suppression in impulsive channels, IEEE Trans. Aerosp. Electron. Syst. 28 (1) (1992) 15–34.
[10] A. Mohammadi, K.N. Plataniotis, Complex-valued Gaussian sum filter for nonlinear filtering of non-Gaussian/non-circular noise, IEEE Signal Process. Lett. 22 (4) (April 2015) 440–444.
[11] P. Chevalier, P. Duvaut, B. Picinbono, Le filtrage de Volterra transverse réel et complexe en traitement du signal, in: Numéro spécial: "Non linéaire et non gaussien", Trait. Signal 7 (5) (1990) 451–476.
[12] P. Chevalier, P. Duvaut, B. Picinbono, Complex transversal Volterra filters optimal for detection and estimation, in: Proc. ICASSP, Toronto (Canada), May 1991.
[13] H. Enzinger, K. Freiberger, G. Kubin, C. Vogel, Fast time-domain Volterra filtering, in: Proc. Asilomar, Pacific Grove, CA USA, Nov. 2016.
[14] M. Schetzen, The Volterra and Wiener theory of non linear systems, Wiley, New-York, 1980.
[15] B. Pincibono, P. Duvaut, Optimal linear quadratic systems for detection and estimation, IEEE Trans. Inf. Theory 34 (March 1988) 304–311.
[16] T. Koh, E.J. Powers, Second order Volterra filtering and its application to non linear system identification, IEEE Trans. Acoust. Speech Signal Process. 33 (6) (Dec. 1985) 1445–1455.
[17] O. Agazzi, D.G. Messerschmitt, D.A. Hodges, Non linear echo cancellation of data signals, IEEE Trans. Commun. 30 (11) (Nov. 1982) 2421–2433.
[18] R.D. Nowak, B.D. Van Veen, Volterra filter equalization: a fixed point approach, IEEE Trans. Signal Process. 45 (2) (Feb. 1997) 377–388.
[19] S. Benedetto, E. Bigieri, R. Daffara, Modeling and performance evaluation of non-linear satellite links – a Volterra series approach, IEEE Trans. Aerosp. Electron. Syst. 15 (July 1979) 494–507.
[20] C. Crespo-Cadenas, M.J. Madero-Ayora, J. Reina-Tosina, J.A. Becerra-Gonzales, Formal deduction of a Volterra series model for complex-valued systems, Signal Process. 131 (2017).
[21] G. Mileounis, N. Kalouptsidis, Blind identification of second-order Volterra systems with complex random inputs using higher order cumulants, IEEE Trans. Signal Process. 57 (10) (Oct. 2009) 4129–4135.
[22] P. Chevalier, B. Picinbono, Complex linear-quadratic systems for detection and array processing, IEEE Trans. Signal Process. 44 (10) (Oct. 1996) 2631–2634.
[23] A. Souloumiac, P. Chevalier, C. Demeure, Improvement in non-Gaussian jammers rejection with a non linear spatial filter, in: Proc. ICASSP, Minneapolis, USA, April 1993, pp. 670–673.
[24] P. Comon, R. Liu, D. Slock, Path-wise wide-sense polynomial receiver for UMTS communications, in: 39th Conf. Com. Contr. Comput., Allerton, Illinois, Oct. 2001.
[25] P. Chevalier, J.-P. Delmas, M. Sadok, Third-order Volterra MVDR beamforming for non-Gaussian and potentially non-circular interference cancellation, IEEE Trans. Signal Process. 66 (18) (Sept. 2018) 4766–4781.
[26] L. Antilla, M. Valkama, Blind signal estimation in widely-linear signal models with fourth-order circularity: algorithms and application to receiver I/Q calibration, IEEE Signal Process. Lett. 20 (3) (March 2013) 221–224.
[27] X. Jiang, W.J. Zeng, A. Yasotharan, H.C. So, T. Kirubarajan, Minimum dispersion beamforming for non-Gaussian signals, IEEE Trans. Signal Process. 62 (7) (April 2014) 1879–1893.
[28] L. Huang, J. Zhang, L. Zhang, Z. Ye, Widely linear minimum dispersion beamforming for sub-Gaussian non-circular signals, Signal Process. 122 (7) (2016) 123–128.
[29] M. Sadok, J.-P. Delmas, P. Chevalier, Enhanced single-antenna interference cancellation from MMSE third-order complex Volterra filters, in: Proc. ICASSP, New-Orleans USA, March 2017.
[30] P. Chevalier, J.-P. Delmas, A. Oukaci, Optimal widely linear MVDR beamforming for noncircular signals, in: Proc. ICASSP, Taipei (Taiwan), April 2009.
[31] P. Chevalier, J.-P. Delmas, A. Oukaci, Properties, performance and practical interest of the widely linear MMSE beamformer for nonrectilinear signals, Signal Process. 97 (April 2014) 269–281.
[32] C. Agne, M.B. Cornell, M. Dale, R. Kearns, F. Lee, Shared-spectrum bandwidth efficient satellite communications, in: 2010 – MILCOM 2010 Military Communication Conference, San Jose, CA, USA, Nov. 2010.
[33] P. Chevalier, L. Albera, A. Ferreol, P. Comon, On the virtual array concept for higher order array processing, IEEE Trans. Signal Process. 53 (4) (April 2005) 1254–1271.
[34] J. Capon, R.J. Greenfield, R.J. Kolker, Multidimensional maximum likelihood processing of a large aperture seismic array, Proc. IEEE 55 (2) (Feb. 1967) 191–211.
[35] P. Chevalier, A. Blin, Widely linear MVDR beamformer for the reception of an unknown signal corrupted by noncircular interferences, IEEE Trans. Signal Process. 55 (11) (Nov. 2007) 5323–5336.
[36] A. Ahmed, A.M. Eltawil, All-digital self-interference cancellation technique for full-duplex systems, IEEE Trans. Wirel. Commun. 14 (7) (July 2015) 3519–3532.
[37] J.-P. Delmas, P. Chevalier, M. Sadok, On the sensitivity of third-order Volterra MVDR beamformers to interference-pulse shaping filter, Signal Process. 170 (May 2020).
[38] I.S. Reed, J.D. Maillet, L.E. Brennan, Rapid convergence rate in adaptive arrays, IEEE Trans. Aerosp. Electron. Syst. AES-10 (6) (Nov. 1974) 853–863.

Mustapha Sadok received the Ph.D. degree in applied mathematics and signal processing from Telecom SudParis, Evry, France, in December 2017. He is currently an Assistant Professor with Institut National des Telecommunications et des TIC d'Oran, Oran, Algeria. His research interests are in signal processing for communications and radio monitoring.

Jean-Pierre Delmas received the M.Sc. degree from Ecole centrale de Lyon, France in 1973, the Certificat d'Etudes Supérieures from Ecole Nationale Supérieure des Télécommunications (ENST), Paris, France in 1982 and the Habilitation diriger des recherches (HDR) degree from the University of Paris XI, Orsay, France in 2001. Since 1980, he has been with Telecom SudParis where he is currently a Professor at the CITI department. He was the deputy director (2005-2010) and the director (2011-2014) of UMR 5157 (CNRS laboratory). His teaching and research interest lie in statistical methods for signal processing with emphasis on asymptotic and non-asymptotic performances analysis and array processing applied to multi-sensor systems in the context of communications. He is author or co-author of more than 140 publications (journal, conference and chapter of book, book). He was an Associate Editor for the IEEE Transactions on Signal Processing (2002-2006) and (2010-2014) for Signal Processing (2009-2020), and currently for IEEE Signal Processing Letters. From 2011 to 2016, he was a member of the IEEE Sensor Array and Multichannel Technical Committee.

Pascal Chevalier received the M.Sc. degree from Ecole Nationale Supérieure des Techniques Avancées, Paris, France, in 1985, the DEA degree in automatic and signal processing from Jussieu university (Paris VII), Paris, France, in 1987, the Ph.D. degree from South-Paris University (Paris XI), Paris, France, in 1991 and the Habilitation Diriger des Recherches degree from Marne-La-Vallée University, Champs-sur-Marne, France, in 2009.

Since 1991, he has been with Thales-Communications-Security (now Thales SIX GTS, France), where he has shared industrial activities, teaching activities both in French engineer schools and French Universities and research activities. Since 2000, he has also been acting as a Technical Manager and an Architect of the array processing subsystem as part of a national program of military satellite telecommunications. He has been a Thales Expert since 2003. Since 2010, he has also been with the Conservatoire National des Arts et Métiers, Paris, France, as a Professor holder of the Electronic Chair. His current research interests include signal processing and array processing techniques for spectrum monitoring and digital communications. He is author or co-author of 30 patents and about 160 publications (Journal, Conferences and Chapters of books). He has been a member of the THOMSON-CSF Technical and Scientifical Council between 1995 and 1998. He co-received the 2003 “Science and Defense” Award from the French Ministry of Defense for its work as a whole about array processing for military radiocommunications. Since 2003, he has been an Associate Editor for EURASIP Journal of Wireless Communications and Networking and Co-technical Chairman of ISWCS’12 Symposium. He is currently a member of the EURASIP Special Area Team related to Signal Processing for Multisensor Systems, a member of the IEEE Sensor Array and Multichannel Technical Committee and an emeritus member of the Societé des Electriciens et des Electroniciens.